

# Phase Equilibria of Bastnaesite, Allanite, and Monazite: Bastnaesite-out Isograds in Metapelites of the Vorontsovskaya Group, Voronezh Crystalline Massif

K. A. Savko and N. S. Bazikov

Voronezh State University, Universitetskaya pl. 1, Voronezh, 394006 Russia

e-mail: ksavko@geol.vsu.ru

Received August 12, 2010; in final form, February 28, 2011

**Abstract**—Paleoproterozoic metapelites of the Vorontsovskaya structure contain accessory REE phosphates (monazite, xenotime, and REE-apatite), fluorine-carbonates (bastnaesite and synchysite), and silicate (allanite). Analysis of phase equilibria involving REE-bearing minerals indicates that bastnaesite is stable only in the greenschist facies and decomposes with the synthesis of monazite at temperatures below the staurolite isograds (490–500°C) at a pressure of 3 kbar. Monazite first appears in the greenschist facies, and its stability expands with increasing temperature, including the granulite facies. A diversity of reaction textures suggests that the mineral is formed in the garnet zone by a reaction of bastnaesite with apatite and by the partial decomposition of REE-bearing chlorite. Monazite is produced in the garnet and staurolite zones by a reaction of allanite with apatite and by a decomposition reaction of REE-bearing apatite.

**DOI:** 10.1134/S0869591111030076

## INTRODUCTION

Accessory minerals attract more and more close attention of petrologists and are often employed in petrological models of geological processes. The mapping of the monazite–allanite and allanite–monazite isograds (Smith and Barero, 1990; Wing et al., 2003; and others) indicates that accessory REE-bearing minerals are not inert in the course of metamorphism but actively participate in prograde metamorphic reactions. Since practically all REE minerals can be dated by isotopic techniques, their involvement in metamorphic reactions provides means for dating the metamorphic processes themselves.

As a widespread accessory mineral of metamorphic rocks, monazite is the most frequently utilized mineralogical geochronometer of metamorphic rocks. The genesis of this mineral was interpreted as follows: it is thought to be produced by the recrystallization of detrital monazite (Rasmussen and Muhling, 2007; Wing et al., 2003) and metamorphic reactions in the greenschist facies (Wing et al., 2003; Savko et al., 2010), when staurolite (Smith and Barero, 1990) and alumino-silicates (Wing et al., 2003) are synthesized. Monazite can also be synthesized by metasomatic processes (Smith et al., 1999) and by the partial melting and recrystallization of earlier monazite (Spear and Pyle, 2002). LREE for monazite synthesis during metamorphism are thought to be borrowed from allanite (Smith and Barero, 1990; Wing et al., 2003), bastnaesite and apatite (Savko et al., 2010), or rock-forming silicates (plagioclase, micas, and chlorite), which can contain

LREE and P in concentrations sufficient for monazite to start growing (Kohn and Malloy, 2004; Carrie and Kohn, 2008). Monazite with or without xenotime can be synthesized at garnet decomposition (Gibson et al., 2004; McFarlane et al., 2005; Kelly et al., 2006). UHT complexes sometimes contain the Ti–LREE silicate perryite ( $\text{La, Ce, Ca}_4(\text{Mg, Fe})_2(\text{Ti, Fe})\text{Si}_4\text{O}_{22}$ ) (Grew and Manton, 1986; Hokada, 2007).

The accessory mineralization found in Paleoproterozoic schists and metasediments of the Vorontsovskaya structure includes REE phosphates (monazite, xenotime, and REE-apatite), F-carbonates (bastnaesite and synchysite), and silicate (allanite). These minerals sometimes occur in reaction relations with one another and with rock-forming minerals. In contrast to other metamorphic complexes, the most widely spread low-temperature REE mineral of these rocks is bastnaesite, which is stable only in the greenschist facies.

This publication is centered on an interpretation of textural relations between accessory REE minerals and on arguments for the occurrence of the isograds of bastnaesite decomposition (*Bst-out*), which coincides with the staurolite isograds in metapelites of the Vorontsovskaya Group.

## GEOLOGY

The eastern Voronezh province (Vorontsovskii graben-synclinorium) separates the Sarmatian segment of the Precambrian crust from the Volga–Ural segment of the East European Platform and has an area of >70 000 km<sup>2</sup> at a width of 100–150 km and a length of

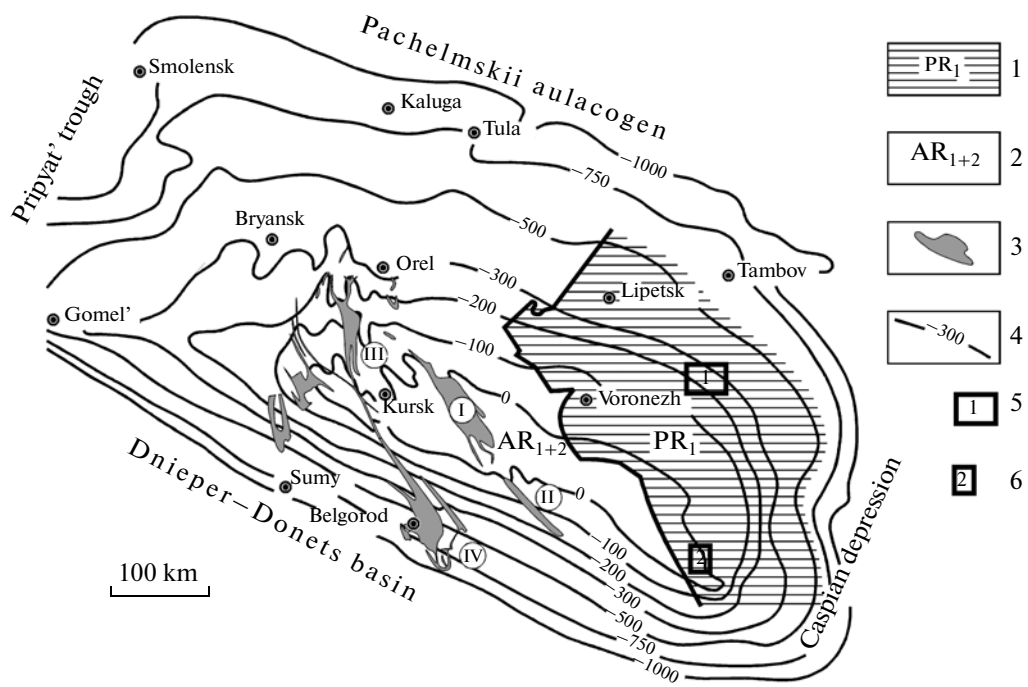


**Fig. 1.** Schematic map showing tectonic zoning of the Precambrian basement of the Voronezh Crystalline Massif (Polyakova et al., 2006). (1) Paleoproterozoic rocks in the eastern part of the Voronezh Crystalline Massif; (2) Archean rocks of the Kursk block; (3) synclinorium structure of the Kursk block filled with Paleoproterozoic rocks (I—Tim-Yastrebovskii, II—Volotovskii, III—Mikhailovskii, IV—Belgorod); (4) isohyps of the Precambrian basement top: areas where metamorphic zoning was mapped: (5) Elan’-Ertil’skii, (6) Mamont-Podkolodnovskii.

>600 km (Fig. 1). The eastern Voronezh province is truncated by the Losevsko-Mamonskii deep fault in the west, with this fault separating the province from the Lipetsk-Losevskii volcanic belt, and is bounded by the Varvarinskii inlier of the Archean basement in the south. The eastern boundary of the province is largely uncertain because of the high thickness of the overlying Phanerozoic sedimentary cover. Judging from seismic data, the thickness of the deposits varies from 2–3 km in the southwestern part to 6–8 km near the Novokhoperskii deep fault. The lithological composition of the group is highly homogeneous: it consists of sandy-shale flyschoid units of the Vorontsovskaya Group intruded by numerous Paleoproterozoic intrusions [syenite dikes of the Artyushkovskii Complex, differentiated massifs of the dunite-peridotite-gabbro association of the Mamonskii Complex ( $2080 \pm 20$  Ma; Chernyshov et al., 1990), pyroxenite-norite-diorite association of the Elan’ Complex ( $2060 \pm 20$  Ma; Chernyshov et al., 1990), S-granitoids of the Bobrovskii Complex ( $2022 \pm 3$  Ma; Bibikova et al., 2009), and gabbro-dolerites of the trap association grouped in the Novogol’skii Complex ( $1805 \pm 14$  Ma; Chernyshov et al., 1990)].

The metasediments of the Vorontsovskaya Group exhibit contrasting variations in their model age values  $T_{\text{Nd}}(\text{DM})$  (from 2.12 to 2.85 Ga), which suggests that

the rocks were formed from the erosion products of both Archean and juvenile Paleoproterozoic sources (Shchipanskii et al., 2007). The U-Pb concordant age of metamorphism [on zircon from crystalline schists of the muscovite-sillimanite zone (Hole 8240)] is  $2104 \pm 4$  Ma (Bibikova et al., 2009). Hence, all intrusions were emplaced into already-metamorphosed rocks of the Vorontsovskaya Group.

## METHODS

All of our samples were taken from borehole core material, which was thoroughly described during fieldwork. Thin sections prepared from the samples were examined under an optical microscope and then under an Jeol 6380 LV electron microscope equipped with an INCA 250 energy-dispersive analytical setup at the Voronezh State University. REE minerals were identified under an optical microscope and in BSE images, their quantitative analyses were conducted using synthetic REE standards (Table 1). The Jeol 6380 LV analyses were conducted at the Voronezh State University at 20 kV accelerating voltage, 1–2 nA absorption current of electrons at Cu, 200 nm beam diameter, and 10 mm focal distance.

Minor and trace elements were analyzed by ICP-MS at the Analytical Certification Test Center of the Insti-

tute of the Problems of Technology of Microelectronics and Superpure Materials, Russian Academy of Sciences. Rock and mineral samples were decomposed in acids in a closed system. The chemical yield at decomposition was controlled using  $^{161}\text{Dy}$ . According to this procedure, the samples were 64–100% dissolved, perhaps, because of the occurrence of insoluble carbonaceous matter, which was visually identified in the form of variable amounts of insoluble black precipitate remaining after the dissolution of the samples. The detection limits were 0.02–0.03 ppm for REE, Hf, Ta, Th, and U; 0.03–0.05 ppm for Nb, Be, and Co; 0.1 ppm for Li, Ni, Ga, and Y; 0.2 ppm for Zr; 0.3 ppm for Rb, Sr, and Ba; and 1–2 ppm for Cu, Zn, V, and Cr. The accuracy of the analyses was controlled by replicate analyses of the SSL-1 Russian standard of metamorphic schist (GSO-3191-85). The relative standard deviation was no greater than 0.3 for all elements at their concentrations of 5 detection limits and no greater than 0.15 at concentrations of >5 detection limits.

#### DESCRIPTION OF ROCKS OF THE VORONTSOVSKAYA GROUP

The Vorontsovskaya Group is composed of metasediments of various types.

The metasandstones are pale gray, fine- to medium-grained, blastopsammitic, massive, or, more rarely, banded rocks with grains ranging from 0.1 to 0.3 mm across (Fig. 2a). The psammitic material is composed of fragments of quartz (up to 55–60%), plagioclase (albite–oligoclase, up to 40%), and single grains of siliceous, quartzite-like, and tuffogenic rocks. Mineral grains are equant, flattened, often with uneven outlines and acute angles. The cement is recrystallized in a microgranoblastic aggregate and consists of quartz, plagioclase, biotite, chlorite, and, occasionally, muscovite.

The schists are gray to dark gray lepidoblastic and porphyroblastic rocks with schistose, banded, and sometimes, crenulated structures. The rocks consist of quartz (30–50%), plagioclase (0–15%), biotite 25–50%), muscovite (0–10%), and subordinate amounts of chlorite, andalusite, carbonaceous matter, and sulfides. Schists in higher temperature metamorphic zones are lepidogranoblastic and granoblastic and contain garnet, staurolite, sillimanite, and greater amounts of muscovite.

The gneisses are gray, medium grained, lepidogranoblastic or granoblastic rocks (Fig. 3c) of gneissose, banded, or crenulated structure and consist of quartz (35–40%), plagioclase (up to 35%), large biotite flakes (5–20%), muscovite (0–15%), garnet (0–5%), sillimanite (3–10%), potassic feldspar (0–5%), and cordierite (0–10%).

The calc-silicate metasediments are greenish-gray granoblastic (with nematogranoblastic features) rocks (Fig. 2d) consisting of quartz, plagioclase (40–50% both), calcite (up to 30%), clinozoisite (up to 25%),

**Table 1.** Standards used for the quantitative analysis of REE-bearing minerals on an Jeol 6380 LV scanning electron microscope equipped with an INCA 250 analytical setup at the Voronezh State University

Element	Standard
Y	Y
La	$\text{LaB}_6$
Ce	$\text{CeO}_2$
Pr	$\text{PrF}_3$
Nd	$\text{NdF}_3$
Sm	$\text{SmF}_3$
Eu	$\text{EuF}_3$
Gd	$\text{GdF}_3$
Tb	$\text{TbF}_3$
Dy	$\text{DyF}_3$
Ho	$\text{HoF}_3$
Yb	$\text{YbF}_3$
Th	$\text{ThO}_2$
U	$\text{UO}_2$

amphibole (10–30%), diopside (up to 10%), garnet (0–5%), and sphene (0–5%).

The chemical composition of metasedimentary rocks of the Vorontsovskaya Group suggests that their protoliths were graywacke–clay sedimentary sequences (Lebedev, 1977).

Metapelites of the Vorontsovskaya Group are characterized by MgO predominance over CaO (except only for rocks in the garnet zone, which bear roughly equal MgO and CaO concentrations) and FeO predominance over  $\text{Fe}_2\text{O}_3$  at a total Fe concentration close to the clarke value (Table 2). The  $\text{K}_2\text{O}/\text{Na}_2\text{O}$  ratios vary between the metamorphic zones. In the garnet zone,  $\text{Na}_2\text{O}$  dominates over  $\text{K}_2\text{O}$ , whereas higher temperature zones always contain more  $\text{K}_2\text{O}$  than  $\text{Na}_2\text{O}$  (Table 2), which is explained by differences in the original lithologies. Because of the medium Fe concentrations of the rocks, the mineral assemblages of the garnet zone with low-temperature garnet occur only in the metamorphosed sandstones (Savko, 1994a), in which plagioclase typically dominates over micas.

The schists contain moderate concentrations of a broad spectrum of minor and trace elements (Table 3), which are close to their average concentrations in Paleoproterozoic graywackes (Condie, 1993).

The total REE concentrations vary from 110 to 260 ppm, as is typical of Precambrian schists. Total LREE concentrations vary from sample to sample

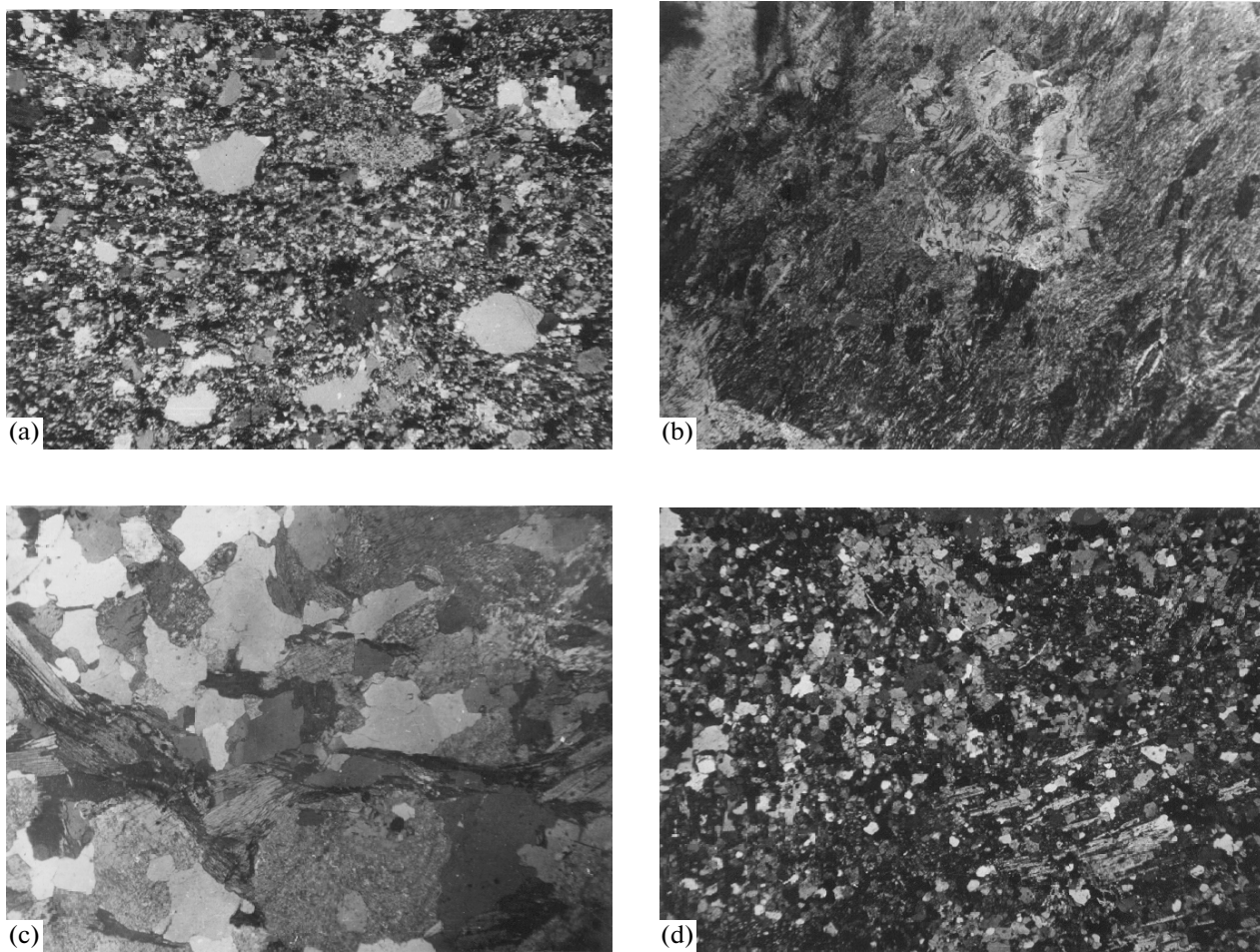


**Fig. 2.** Types of rocks of the Vorontsovskaya Group. (a) Blastopsammitic biotite–feldspar–quartz metasandstone. Crossed polarizers, magnification 24×, sample 8305/276. (b) Graphite-bearing schist with staurolite porphyroblasts replaced by muscovite in the margins. One polarizer, magnification 10×, sample 8286/466. (c) Muscovite–biotite gneiss. Crossed polarizers, magnification 15×, sample 8354/378. (d) Calc–silicate metasedimentary calcite–amphibole–clinozoisite–plagioclase–quartz rock. Crossed polarizers, magnification 20×, sample 8312/342.

from 98 to 232 ppm. The chondrite-normalized REE patterns (Fig. 3a) have negative Eu anomalies [ $\text{Eu}/\text{Eu}^* = \text{Eu}_n/(\text{Sm}_n + \text{Gd}_n)0.5 = 66–0.87$ ], except only a single sample (whose  $\text{Eu}/\text{Eu}^* = 1.21$ ) and steep negative slopes [ $(\text{La/Yb})_n = 7.3–13.1$ ,  $(\text{Gd/Yb})_n = 1.22–2.17$ , and  $(\text{LREE/HREE})_n = 2.44–3.66$ ] (Table 3). These features are typical of post-Archean clay shales, whose protoliths consisted of detrital material with erosion products of granitic rocks (Likhmanov et al., 2008).

The  $\text{Ce}/\text{Ce}^*$  ratio [where  $\text{Ce}/\text{Ce}^* = \text{Ce}_n/(\text{Ln}_n + \text{Pr}_n)0.5$ ] of the carbonaceous schists is 0.97–1.10, which suggests [with regard for  $(\text{LREE/HREE})_n = 2.44–3.66$ ] that the sediments were accumulated on the shelf, in a humid climate, and a quiescent tectonic environment (Balashov, 1976; Murray et al., 1990).

The Th/U ratio of schists of the Vorontsovskaya Group varies from 2.47 to 4.41, except only one sam-

ple of carbonaceous schist (sample 8384/430), whose  $\text{Th}/\text{U} = 1.24$ . These values suggest that the material was supplied to the sedimentation basin from a mixed source, which involved weathering products of volcanic rocks (greenstone belts) with  $\text{Th}/\text{U} < 3$  and granitic rocks with  $\text{Th}/\text{U} > 4$  (McLennan et al., 1995). This also follows from the elevated concentrations of both lithophile and siderophile elements (high concentrations of Cr and Ni) (Table 3), which suggest a mixed (basite and silicic) source (Shchipanskii et al., 2007). The predominant components of these sources should have been volcanics of the Losevskaya Formation and Usmanskii granitoids (Shchipanskii et al., 2007).

The REE concentrations of biotite and muscovite from the staurolite (sample 8712/4), staurolite–sillimanite (samples 8713/1 and 8715/2), and muscovite–sillimanite (sample 8371/488) zones are generally

**Table 2.** Chemical composition (wt %) of rocks of the Vorontsovskaya Group

Com- ponent	Garnet zone					Staurolite zone					Staurolite— sillimanite zone			Muscovite— sillimanite zone			
	8305/ 275	8200/ 209	8062/ 380	8617/ 404	8600/ 307.9	8307/ 334	8286/ 499	8287/ 273	8309/ 339.4	8712/ 506.5	8758/ 562	8713/ 634.4	8312/ 304.8	8384/ 300	8240/ 352	8371/ 365	8282/ 386.8
SiO <sub>2</sub>	65.80	68.28	60.30	65.30	66.78	69.22	59.32	57.94	59.40	60.24	55.72	59.40	65.76	55.86	65.54	59.4	54.20
TiO <sub>2</sub>	0.52	1.02	1.04	0.96	0.45	0.87	0.97	1.30	1.08	0.80	0.90	0.40	0.90	1.02	0.48	0.90	0.77
Al <sub>2</sub> O <sub>3</sub>	13.85	13.12	16.12	13.90	14.13	12.72	14.35	17.11	15.97	18.64	17.25	19.56	14.16	17.12	13.48	17.10	19.61
Fe <sub>2</sub> O <sub>3</sub>	1.37	0.85	2.70	1.64	1.26	1.26	3.80	3.06	2.13	0.88	2.16	2.63	0.76	2.83	2.93	1.41	2.00
FeO	5.39	4.11	3.60	3.89	4.89	4.70	4.18	4.43	5.98	5.69	7.33	6.20	4.50	5.91	4.85	6.39	7.48
MnO	0.07	0.05	0.02	0.02	0.04	0.03	0.08	0.06	0.04	0.02	0.11	0.05	0.06	0.08	0.39	0.10	0.08
MgO	2.85	2.17	2.90	2.92	2.25	2.25	3.30	4.19	3.52	2.84	4.31	2.82	2.90	3.54	3.03	3.56	4.45
CaO	2.76	2.74	3.08	3.49	1.79	1.59	2.85	1.37	1.37	1.65	1.93	0.70	5.70	1.94	1.68	2.53	1.38
Na <sub>2</sub> O	4.00	2.90	3.00	3.37	3.30	1.50	2.20	0.40	1.90	2.10	2.70	1.75	1.20	2.20	1.80	2.40	2.10
K <sub>2</sub> O	1.90	2.00	3.70	2.40	2.00	3.10	2.10	4.20	3.40	3.60	2.80	3.80	1.45	4.40	3.80	3.65	4.65
LOI	1.54	2.03	2.58	2.34	1.22	3.00	5.88	5.35	4.04	2.21	3.26	2.97	1.66	4.52	2.99	1.58	2.56
P <sub>2</sub> O <sub>5</sub>	0.14	0.23	0.53	0.16	0.12	0.21	0.23	0.21	0.16	0.13	0.11	0.12	0.37	0.21	0.31	0.21	0.19
Total	100.19	99.50	99.57	100.39	98.23	100.45	99.26	99.62	99.09	98.80	98.58	100.40	99.30	99.63	100.92	99.23	99.47
H <sub>2</sub> O <sup>-</sup>	—	0.04	0.24	1.28	0.23	0.43	0.05	0.17	0.40	0.10	0.10	0.07	0.14	0.17	0.18	n.d.	0.20
SO <sub>3</sub>	0.06	0.09	0.35	0.15	0.04	0.62	3.17	3.35	0.12	0.13	0.14	0.46	0.07	1.38	0.62	0.46	0.77

lower than in the rocks (Table 4, Fig. 3b). The minimum concentrations (of the order of a few ppm) were detected in muscovite from the high-temperature muscovite–sillimanite zone (Fig. 3b). The high concentrations of Y (562 ppm), Zr (903 ppm), and all HREE (210 ppm) (Table 4, Fig. 3b) indicate that garnet concentrates these elements.

## METAMORPHISM

The zonal metamorphism of rocks in the eastern Voronezh province was studied within isolated domains in the Elan’–Ertiškii and Mamon–Podkolodnovskii areas (Savko, 1990, 1994b; Savko and Gerasimov, 2002; Gerasimov and Savko, 1995) as thoroughly as possible in a poorly exposed region drilled with merely a thin network of boreholes. The garnet (430–480°C), staurolite (490–520°C), staurolite–sillimanite (520–560°C), and muscovite–sillimanite (560–600°C) zones were mapped in the Elan’–Ertiškii area (Fig. 4a), whose metamorphism did not reach the conditions of the highest temperature sillimanite–potassic feldspar–cordierite zone. No metapelites of the lowest temperature garnet zone were found in the Mamon–Podkolodninskii area, which contains highest temperature rocks of the Vorontsovskaya Group: garnet–sillimanite–cordierite

gneisses (600–750°C) (Fig. 4b). The metamorphic pressures varied from 3 kbar in the garnet zone to 5 kbar in the garnet–sillimanite–cordierite zone.

**Garnet zone.** In the field of the Vorontsovskaya Group, metasediments of the garnet zone are exposed within three isolated domains. The largest of them extends from the northeastern part of the Elan’ pluton eastward toward the Novokhoperskaya zone and has a width of 8–18 km (Fig. 4a). Another domain occurs between the Elan’ and Talovskii intrusions, trends to the northwest, and has a maximum width of 10 km. Conceivably, this domain is connected with the first (the largest) one, but it is hard to determine this for sure because the regionally metamorphosed rocks are overprinted with the contact aureole of the Elan’ Massif. The third domain is very small and corresponds to a local metamorphic temperature minimum within the staurolite zone. The most widely spread mineral assemblages are *Qtz + Ab + Bt + Chl + Ms*, *Qtz + Pl + Chl + Bt*, *Qtz + Bt + Chl*, and *Qtz + Ab + Bt + Grt*.<sup>1</sup>

<sup>1</sup> Mineral symbols: *Ab*—albite, *Ahn*—allanite, *And*—andalusite, *Ae*—apatite, *Bst*—bastnaesite, *Bt*—biotite, *Cal*—calcite, *Chl*—chlorite, *Cpy*—chalcopyrite, *Crd*—cordierite, *Grt*—garnet, *Ilm*—ilmenite, *Kfs*—potassium feldspar, *Mnz*—monazite, *Ms*—muscovite, *Pl*—plagioclase, *Po*—pyrrhotite, *Py*—pyrite, *Qtz*—quartz, *Rut*—rutile, *Sph*—sphene, *Sil*—sillimanite, *Spl*—spinel, *St*—staurolite.

**Table 3.** Concentrations (ppm) of minor and trace elements in metamorphic rocks of the Vorontsovskaya Group

Element	7522/308a	8186/400	8197/452	8384/430b	8731/402.5	8715/427.5	548c
Li	69.27	27.72	53.50	36.73	24.02	211.68	61.46
Be	1.46	0.86	1.30	1.66	1.04	3.00	1.69
Sc	15.47	7.42	13.80	10.06	9.28	12.30	15.89
V	162.97	105.25	130.73	190.75	97.06	126.10	149.66
Cr	140.06	122.76	127.69	203.98	103.27	96.04	152.03
Co	22.37	16.11	16.96	28.07	13.74	21.88	18.28
Ni	71.01	51.59	58.33	77.70	54.34	69.43	61.54
Cu	93.35	53.85	38.68	182.22	40.48	135.25	90.28
Zn	111.90	59.85	104.25	108.92	73.30	76.50	94.35
Ga	23.05	15.42	20.12	17.32	15.36	23.16	18.41
As	3.13	8.87	bdl	8.55	3.94	0.83	0.51
Se	<1.3	<1.5	<1.5	4.44	<1.5	<3	<0.6
Rb	119.41	76.66	142.56	151.75	83.62	105.32	107.11
Sr	288.83	146.47	169.01	104.59	211.63	329.85	261.84
Y	19.01	17.77	17.83	13.96	14.58	35.72	19.65
Zr	122.93	247.45	146.92	136.07	195.34	246.08	119.44
Nb	9.77	9.45	10.48	17.08	8.79	12.51	8.31
Mo	2.84	2.87	0.63	20.07	0.95	1.43	2.60
Ag	0.22	0.16	0.08	1.21	0.18	0.27	0.21
Sn	1.70	1.92	2.12	5.07	1.86	1.50	2.28
Sb	1.20	0.74	0.82	2.63	0.69	0.26	0.36
Cs	6.68	2.27	10.99	14.73	4.11	17.34	6.74
Ba	641.52	405.61	402.05	264.03	367.02	125.36	674.12
La	34.36	28.52	28.46	32.32	25.01	55.82	29.44
Ce	76.50	55.63	57.75	60.79	52.40	108.59	66.12
Pr	8.46	6.33	7.00	6.55	6.29	12.23	7.25
Nd	32.14	24.74	27.48	25.16	23.99	46.24	28.45
Sm	6.20	4.48	5.27	4.34	4.33	8.80	5.11
Eu	1.26	1.07	1.10	0.99	1.08	2.29	1.27
Gd	4.96	4.13	4.47	3.43	3.63	8.28	4.17
Tb	0.77	0.64	0.72	0.55	0.59	1.25	0.63
Dy	3.53	3.21	3.57	2.66	2.94	6.71	3.41
Ho	0.70	0.66	0.72	0.51	0.62	1.31	0.69
Er	2.06	2.02	2.14	1.49	1.87	3.81	1.86
Tm	0.30	0.29	0.32	0.24	0.27	0.55	0.27
Yb	1.96	1.93	2.06	1.67	1.90	3.72	1.80
Lu	0.28	0.28	0.30	0.24	0.27	0.54	0.26
Hf	3.42	6.37	4.24	3.43	5.08	7.00	3.56
Ta	0.79	0.91	0.93	1.26	0.82	1.30	0.82
W	2.76	3.02	1.09	4.19	2.11	1.40	0.99
Tl	0.53	0.28	0.60	2.15	0.46	0.43	0.56
Pb	19.66	10.71	10.02	24.44	11.12	29.58	10.78
Bi	0.24	0.09	0.11	0.90	0.09	0.34	0.13
Th	5.82	5.52	6.03	7.12	4.64	10.93	5.41
U	1.95	1.68	1.75	5.72	1.41	3.56	2.11
ΣREE	173.48	133.93	141.35	140.94	125.18	260.12	150.73
Ce/Ce*	1.07	0.97	0.97	0.97	1.00	0.97	1.08
Eu/Eu*	0.67	0.75	0.68	0.76	0.81	0.81	0.82
(La/Yb) <sub>n</sub>	12.58	10.61	9.90	13.89	9.46	10.78	11.74
(Gd/Yb) <sub>n</sub>	2.09	1.77	1.79	1.70	1.58	1.84	1.92
(LREE/HREE) <sub>n</sub>	3.35	2.87	2.80	3.66	2.85	2.79	3.16
La/Sc	2.22	3.85	2.06	3.21	2.69	4.54	1.85
Th/Sc	0.38	0.74	0.44	0.71	0.50	0.89	0.34
La/Th	5.91	5.17	4.72	4.54	5.39	5.11	5.44
Co/Th	3.85	2.92	2.81	3.95	2.96	2.00	3.38
Th/U	2.98	3.28	3.45	1.24	3.28	3.07	2.57

**Table 3.** (Contd.)

Element	583c/3	809/19	831/6	7308**	7219**	249**	834**
Li	56.28	49.00	58.39	n.d.	n.d.	n.d.	n.d.
Be	1.73	1.54	1.84	n.d.	n.d.	n.d.	n.d.
Sc	16.91	16.45	11.04	16.88	16.26	12.27	12.67
V	185.47	168.64	132.87	138.60	94.43	96.31	94.45
Cr	168.55	184.66	103.89	126.60	103.40	94.62	114.80
Co	19.78	21.00	16.16	22.03	16.35	14.38	14.79
Ni	68.63	65.84	45.29	96.57	54.41	62.38	63.94
Cu	62.71	75.15	55.30	n.d.	n.d.	n.d.	n.d.
Zn	103.82	108.83	106.33	n.d.	n.d.	n.d.	n.d.
Ga	20.10	18.80	21.97	n.d.	n.d.	n.d.	n.d.
As	5.01	1.09	0.34	n.d.	n.d.	n.d.	n.d.
Se	<2	<0.7	<1.4	n.d.	n.d.	n.d.	n.d.
Rb	100.04	116.10	154.79	107.70	95.35	70.58	80.22
Sr	220.01	255.92	106.24	228.00	285.00	293.00	402.00
Y	23.78	17.24	19.40	19.74	24.85	14.97	16.69
Zr	145.54	162.80	181.35	149.40	160.50	141.80	200.20
Nb	9.73	9.41	11.66	8.62	8.77	7.17	6.49
Mo	3.90	4.53	9.84	n.d.	n.d.	n.d.	n.d.
Ag	0.17	0.15	0.18	n.d.	n.d.	n.d.	n.d.
Sn	4.49	2.74	2.82	n.d.	n.d.	n.d.	n.d.
Sb	0.58	0.42	0.52	n.d.	n.d.	n.d.	n.d.
Cs	5.62	6.16	6.75	n.d.	n.d.	n.d.	n.d.
Ba	1072.15	620.72	969.66	498.00	468.00	337.00	533.00
La	36.68	25.10	32.21	28.28	25.25	21.99	22.30
Ce	77.89	53.72	67.76	62.94	53.44	46.18	48.57
Pr	8.18	6.19	6.58	6.41	6.41	5.41	5.93
Nd	32.78	23.96	25.81	29.77	24.30	20.98	23.98
Sm	5.47	4.39	4.64	5.55	4.52	3.89	4.20
Eu	1.27	1.00	0.98	1.12	1.17	1.44	1.10
Gd	4.73	3.68	3.86	4.60	3.64	3.23	3.31
Tb	0.73	0.57	0.60	0.65	0.58	0.47	0.48
Dy	3.86	2.94	3.48	3.58	3.57	2.61	2.85
Ho	0.74	0.57	0.69	0.70	0.81	0.51	0.59
Er	2.18	1.66	1.96	1.91	2.37	1.34	1.63
Tm	0.32	0.24	0.29	0.28	0.38	0.19	0.24
Yb	2.00	1.65	1.91	1.83	2.47	1.23	1.44
Lu	0.28	0.25	0.29	0.28	0.38	0.20	0.22
Hf	4.43	4.84	5.68	4.08	4.14	3.80	5.15
Ta	1.08	0.96	1.28	0.68	0.73	0.50	0.46
W	1.35	0.93	2.14	n.d.	n.d.	n.d.	n.d.
Tl	0.64	0.54	0.65	n.d.	n.d.	n.d.	n.d.
Pb	15.52	11.55	13.53	11.21	9.47	12.52	10.09
Bi	0.16	0.21	0.36	n.d.	n.d.	n.d.	n.d.
Th	6.92	6.36	8.65	6.74	5.16	5.03	4.04
U	2.47	2.25	3.51	1.53	1.37	1.20	1.03
$\Sigma$ REE	177.12	125.92	151.05	147.90	129.29	109.67	116.84
$\Sigma$ LREE	161.01	113.36	136.99	132.95	113.92	98.45	104.98
Ce/Ce*	1.06	1.03	1.08	1.10	1.00	1.01	1.01
Eu/Eu*	0.75	0.74	0.69	0.66	0.85	1.21	0.87
(La/Yb) <sub>n</sub>	13.13	10.94	12.07	11.08	7.33	12.82	11.11
(Gd/Yb) <sub>n</sub>	1.95	1.85	1.67	2.08	1.22	2.17	1.90
(LREE/HREE) <sub>n</sub>	3.36	3.05	3.25	3.00	2.44	2.87	2.97
La/Sc	2.17	1.53	2.92	1.68	1.55	1.79	1.76
Th/Sc	0.41	0.39	0.78	0.40	0.32	0.41	0.32
La/Th	5.30	3.95	3.72	4.20	4.89	4.37	5.52
Co/Th	2.86	3.30	1.87	3.27	3.17	2.86	3.66
Th/U	2.80	2.82	2.47	4.41	3.77	4.19	3.92

\*\* Compiled from (Shchipanskii et al., 2007).

**Table 4.** Concentrations (ppm) of minor and trace elements in silicate minerals from metamorphic rocks of the Vorontsovskaya Group

Element	8712/4	8715/2	8713/1			8371/488	
	Bt	Bt	Bt	Ms	Grt	Bt	Ms
Li	1544	1045	1246	322	37.3	363	1140
Be	0.12	0.43	0.66	0.21	0.21	0.70	6.8
Sc	48.4	52.3	45.6	22.8	120	44.0	30.1
V	321	418	466	284	61.5	378	13.9
Cr	343	919	1066	1113	146	327	14.2
Co	63.6	59.4	56.7	61.2	16.2	42.7	0.57
Ni	233	232	204	225	15.2	115	2.3
Cu	27.6	83.3	15.8	14.7	4.1	16.9	5.4
Zn	350	340	362	409	92	409	100
Ga	44.5	35.2	37.6	41.1	13.9	35.6	105
As	1.2	9.7	2.2	2.1	1.2	2.8	0.89
Se	bdl	<1	bdl	<1.2	<15	bdl	bdl
Rb	434	360	289	9.7	9.5	357	915
Sr	11.0	8.5	9.4	16.0	7.9	9.6	7.6
Y	13.4	23.3	17.8	30.2	561.9	6.6	8.1
Zr	108	99.1	126	136	903	164	100
Nb	24.1	27.8	23.2	5.2	1.4	27.0	115
Mo	0.29	1.2	0.95	0.43	0.39	0.31	0.53
Rh	bdl	bdl	bdl	bdl	bdl	bdl	bdl
Pd	bdl	bdl	bdl	bdl	bdl	bdl	bdl
Ag	1.5	1.2	1.8	1.4	1.4	0.48	3.6
Cd	bdl	bdl	bdl	bdl	0.83	0.45	bdl
Sn*	13.6	13.0	8.5	2.9	1.2	4.4	59.4
Sb	0.32	0.51	0.52	0.54	0.37	1.1	0.15
Te	bdl	bdl	bdl	bdl	bdl	bdl	bdl
Cs	148	69.9	102	3.3	0.7	28.1	38.7
Ba	1228	1997	1912	76.7	123	1496	22.9
La	15.9	27.8	15.3	19.8	20.1	23.0	1.8
Ce	34.9	59.9	34.0	46.8	41.9	50.4	4.4
Pr	4.2	7.2	3.9	5.5	5.2	6.1	0.53
Nd	16.6	25.9	14.9	21.1	19.2	22.5	2.1
Sm	3.3	4.8	3.0	4.1	4.9	3.9	0.68
Eu	0.37	0.21	0.23	0.39	0.82	0.15	0.016
Gd	2.8	3.8	2.8	3.9	18.6	2.9	0.87
Tb	0.45	0.68	0.51	0.73	5.6	0.4	0.18
Dy	2.3	3.3	2.8	4.4	56.7	1.4	1.0
Ho	0.49	0.74	0.64	1.1	14.9	0.24	0.24
Er	1.4	2.4	1.9	3.1	52.1	0.62	0.72
Tm	0.21	0.35	0.26	0.46	8.1	0.09	0.11
Yb	1.4	2.3	1.8	2.9	55.4	0.67	0.76
Lu	0.22	0.35	0.27	0.43	7.2	0.10	0.10
Hf	2.7	2.5	3.0	3.2	17.1	4.0	2.4
Ta	1.8	2.2	1.8	0.52	0.27	2.2	9.1
W	0.54	1.0	0.60	0.30	0.37	1.0	7.3
Re	bdl	bdl	bdl	bdl	<0.04	bdl	bdl
Ir	bdl	bdl	bdl	bdl	<0.08	bdl	bdl
Pt	bdl	bdl	<0.06	<0.06	<0.2	<0.1	bdl
Au	bdl	bdl	bdl	bdl	bdl	bdl	bdl
Tl	1.9	1.5	1.2	0.059	0.057	1.6	3.1
Pb	7.1	6.9	4.8	5.2	6.4	7.7	3.7
Bi	0.29	0.17	0.13	0.084	0.073	0.43	0.094
Th	4.5	6.2	3.9	4.5	4.7	6.5	2.5
U	1.2	1.3	1.2	1.7	3.1	1.5	2.5

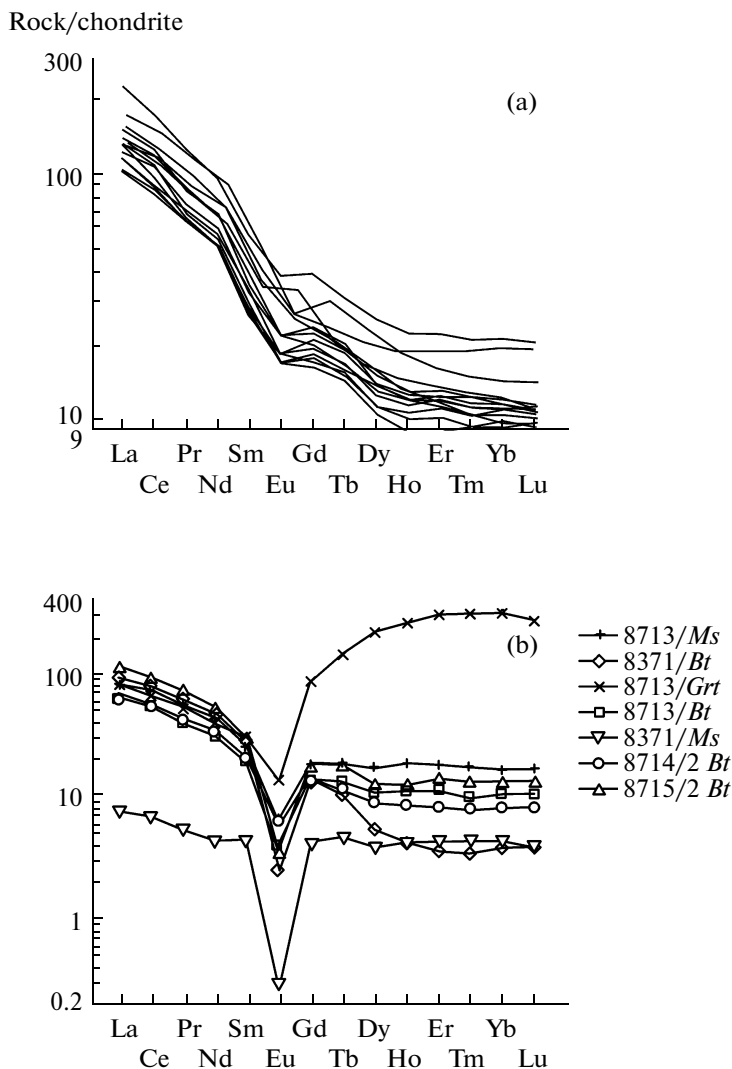


**Fig. 3.** Chondrite-normalized REE patterns. (a) Metamorphic rocks of the Vorontsovskaya Group. (b) Minerals from schists of the Vorontsovskaya Group.

**Staurolite zone.** Metapelites of the staurolite zone are widespread in the eastern part of the Voronezh Crystalline Massif and occur in the central part of the Vorontsovskaya structure (in the Elan’–Ertiš’kii zone) and in its southern part (in the Mamon–Podkolodnovskii zone). The metasediments of the staurolite zone are plagioclase–quartz–biotite schists and metasandstones, which often contain staurolite, garnet, andalusite, muscovite, and chlorite. Staurolite most often appears at the lowest temperatures in the recrystallized matrix of metasandstones, which are slightly more ferrous than the schists. The mineral assemblages of the staurolite zone depend on the temperature and pressure regime and on the chemical composition of the rocks. The smallest number of degrees of freedom has the assemblage  $Qtz + Bt + Pl \pm St \pm Ms \pm Grt \pm And \pm Chl$ .

**Staurolite–sillimanite zone.** In the Elan’–Ertiš’kii tectonic zone, a staurolite–sillimanite metamorphic zone was mapped as a sublatitudinal stripe 5–9 km wide, which sometimes branches. Fields of this zone of other geometry were mapped in the area of the Talovskii gabbro–diorite massif and the Elan’ gabbroid massif. In the southern part of the Vorontsovskaya structure (Mamon–Podkolodnovskii field), a staurolite–sillimanite zone was mapped as a semicircular stripe 2–8 km wide around metasediments of the muscovite–sillimanite zone. The main mineral assemblage of this zone is  $Qtz + Pl + Ms + Sil + St + Grt + Bt$ .

The **muscovite–sillimanite zone** is widespread in zonal metamorphic complexes of moderate pressure, but in contrast to the other zones (staurolite, staurolite–sillimanite, and sillimanite–potassic feldspar–cordierite), this zone contains mineral assemblages with very small numbers of minerals. Three relatively

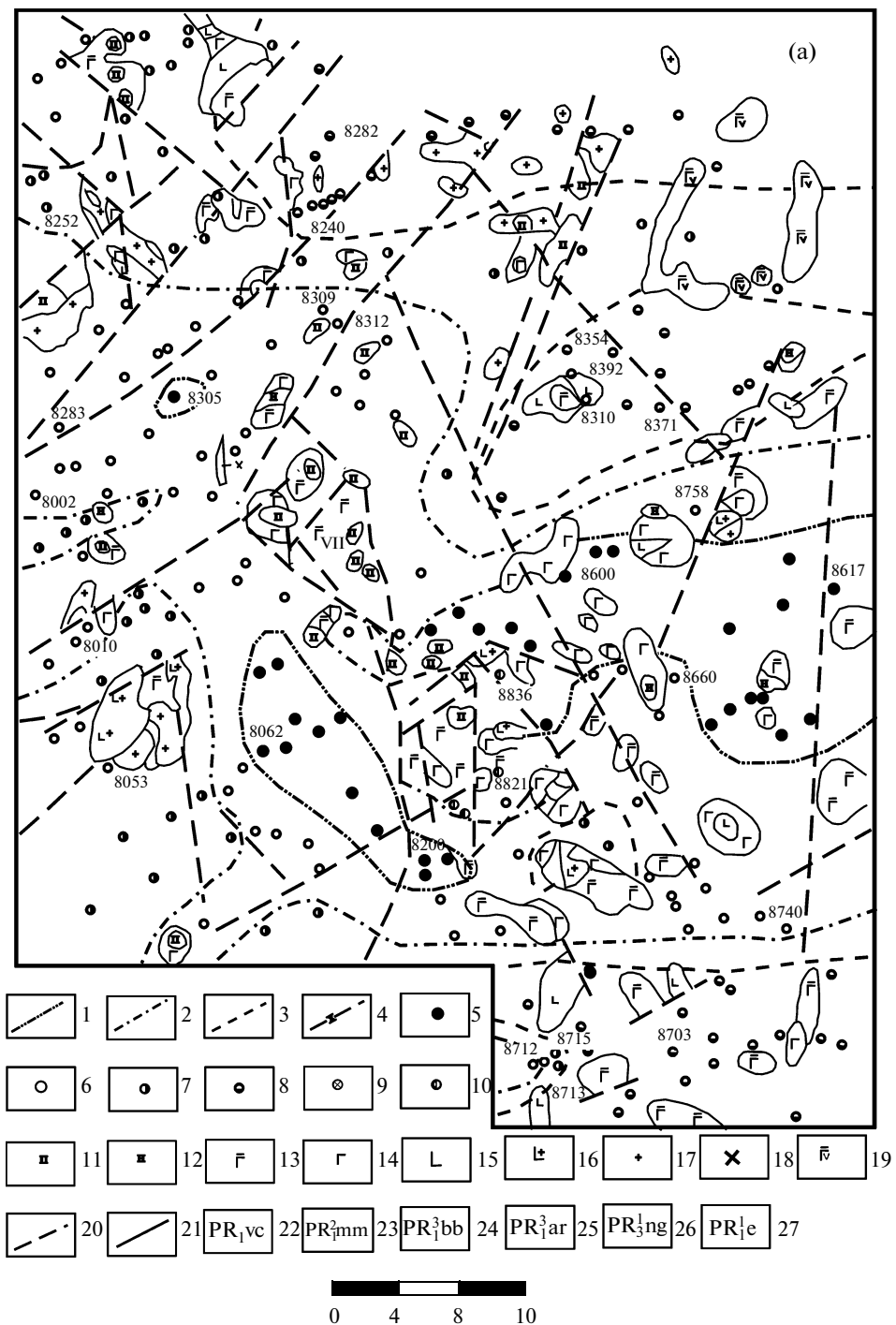


**Fig. 4.** Metamorphic zoning of the Vorontsovskaya Group: (a) Vorontsovskaya Group; (b) Mamon-Podkolodnovskii area. Iso-grade: (1) staurolite, (2) staurolite-sillimanite, (3) sillimanite, (4) sillimanite-potassic feldspar-cordierite. Sampling sites of rocks with mineral assemblages of (5) garnet zone, (6) staurolite zone, (7) staurolite-sillimanite zone, (8) muscovite-sillimanite (9) sillimanite-potassic feldspar-cordierite zone, (10) metapelitic xenoliths in magmatic rocks. Intrusive rock, Mamonskii Complex: (11) peridotites, (12) pyroxenites, (13) gabbro-norites; Elan' Complex: (14) norites, (15) diorites; Bobrovskii Complex: (16) granodiorites and quartz diorites, (17) granites; Artyushkinskii Complex: (18) syenites; Novogol'skii Complex: (19) gabbro-dolerites; (20) faults; (21) geological boundaries. Symbols: (22) Vorontsovskaya Group, (23) Mamonskii Complex; (24) Bobrovskii Complex, (25) Artyushkinskii Complex; (26) Novogol'skii Complex; (27) Elan' Complex.



Fig. 4. (Contd.)

large fields of rocks of the muscovite–sillimanite zone were mapped in the Elan’–Ertiškii domain. Metapelites of the muscovite–sillimanite zone are a predominant rock type in the metamorphic zoning of the Mamon–Podkolodnovskii domain. These rocks are exposed as a semicircular stripe 7–12 km wide around the highest temperature biotite–potassic feldspar–cordierite gneisses. The rocks contain a rela-

tively little diverse mineral assemblages, and the smallest number of degrees of freedom has the assemblage  $Qtz + Pl + Bt + Ms + Grt + Sil \pm Kfs$ .

**Sillimanite–potassic feldspar–cordierite zone.** The metamorphic zoning of the Mamon–Podkolodnovskii domain includes metapelites of the highest temperature zone only in the southern part of the area. These rocks were mapped as an almost oval field 13 × 17 km

of sillimanite–cordierite gneisses (Fig. 4b). It is bounded by a gabbro–diorite semicircular intrusion in the west, a small peridotite massif in the north, and a field of metapelites of the muscovite–sillimanite zone in the east. The southern boundary of the zone is uncertain because that area was not drilled. The field of the sillimanite–cordierite gneisses was determined to be intruded by numerous small hyperbasite bodies. The metapelites of this zone are medium-grained biotite–sillimanite gneisses, which often contain cordierite, garnet, potassic feldspar, and spinel and have granoblastic or lepidogranoblastic textures. The most widely spread mineral assemblage are  $Qtz + Pl + Bt + Sil \pm Kfs \pm Crd \pm Grt \pm Sp + Ilm \pm Po$ . Although occasional samples contain garnet, cordierite, and potassic feldspar, these minerals have never been found in contact, and hence, no higher temperature garnet–orthoclase–cordierite zone was distinguished in the area.

### MINERALOGY OF THE REE-BEARING MINERAL PHASES

The associations of both rock-forming and accessory REE-bearing minerals in metasedimentary rocks of the Vorontsovskaya Group are listed in Table 5 (according to metamorphic zones), which shows that bastnaesite is contained only in the garnet zone, allanite was found only in the staurolite zone, xenotime occurs predominantly in the staurolite–sillimanite zone, while monazite and apatite are contained in all of the metamorphic zones.

**Allanite**  $CaREEAl_2Fe^{2+}Si_3O_{11}O(OH)$  is an REE-bearing silicate of the epidote group and was identified in two samples from the staurolite metamorphic zone. In sample 8712/4, allanite occurs as an elongated grain (15  $\mu m$  long) in contact with monazite (Fig. 5a) and as small grains approximately 5  $\mu m$  across. At the boundary between allanite and monazite, a small grain of REE-bearing apatite was detected. REE contained in the allanite are dominated by Ce (the mineral contains 12.30–13.59 wt %  $Ce_2O_3$ ), whose concentration is almost three times higher than those of La (4.62–5.76 wt %  $La_2O_3$ ) and Nd (3.83–5.04 wt %  $Nd_2O_3$ ) (Table 6); the mineral also contains Th (1.65–2.26 wt %  $ThO_2$ ) and Pr (0.72–0.91 wt %  $Pr_2O_3$ ). The allanite grains display a zonal Ce and La distribution, with an increase in their concentrations from grain cores to margins, and with Nd and Th showing the opposite trends (Table 6). The mineral also contains P, whose concentration increases from 0.10 wt %  $P_2O_5$  in the core to 0.92 wt % in the margin (Table 6).

Small allanite grains (less than 5  $\mu m$ ) were found in sample 8010/287 (Fig. 5b) from the low-temperature part of the staurolite zone. The mineral occurs in this rock in association with large (up to 50  $\mu m$ ) monazite grains and REE-bearing apatite. This allanite contains much less REE (almost three times less) than the mineral in sample 8712/4 and contains no Th. REE are

dominated by Ce (4.51 and 6.46 wt %  $Ce_2O_3$ ), and the concentrations of La (1.68 and 2.37 ppm  $La_2O_3$ ) and Nd (2.21 and 2.73 wt %  $Nd_2O_3$ ) are lower (Table 6).

**Monazite** ( $REEPO_4$ ) is the most widely spread accessory REE-bearing mineral and was identified in most of our samples with REE mineralization. Nevertheless, some samples from the lowest temperature metapelites (from the garnet zone) either contain no monazite at all or, if present, this mineral occurs in association with bastnaesite or in reaction relations with apatite, chlorite, and biotite (Table 5). Starting in the staurolite zone, monazite is contained in all samples. Monazite occurs in the garnet and staurolite zones as small (no larger than 20  $\mu m$ ) unzoned grains. The higher temperature rocks (from the muscovite–sillimanite and sillimanite–cordierite–potassic feldspar zones) contain larger monazite grains (up to 100–150  $\mu m$ ) (Fig. 6a).

Reaction textures with REE-bearing minerals are widespread in the garnet zone and occur not as widely in the staurolite zone. Monazite and allanite were detected only in two samples from the staurolite zone, in which they occur in close association with apatite (Table 5). Monazite sometimes occurs in contact with bastnaesite and in the presence of apatite (Fig. 5c). In samples 8200/209 and 7004/264, very small monazite grains are included in bastnaesite (Figs. 5d, 5e). Relations between monazite and apatite (which often contains REE) are diverse: in the garnet zone, these are numerous irregularly shaped monazite inclusions in apatite (Fig. 5f), tiny monazite lamellas along cleavage planes in apatite (Fig. 7a), and rims round pyrite (Fig. 7f). In some samples from the garnet zone, numerous small monazite grains replace large crystals of chlorite (Figs. 7c–7e) and biotite, together with bastnaesite (Fig. 5d).

No differences were detected between the chemical compositions of monazite from different metamorphic zones (Table 7). The mineral always contains much Ce and minor admixtures of Ca and Si.

REE are dominated by Ce (28–32 wt %  $Ce_2O_3$ ), and the mineral contains much La and Nd (12–15 wt %  $La_2O_3$  and  $Nd_2O_3$  each) and Pr (2–5 wt %  $Pr_2O_3$ ). The HREE contained in the monazite are Sm, Gd (1–3.5 wt %  $Sm_2O_3$  and  $Gd_2O_3$  each), and Eu (up to 2 wt %  $Eu_2O_3$ ). Along with REE, the monazite contains Th, U, Pb (2–5 wt %  $ThO_2$  and 0.5–1 wt %  $PbO$  and  $UO_3$  each), and minor amounts of Ca and Si (Table 7). The P concentration in the mineral almost exactly corresponds to the stoichiometric value. It is interesting that monazite from various metamorphic zones may contain up to 1.5 wt % F.

The fact that the monazite contains Pb (up to 1 wt %  $PbO$ ) is explained by the generation of this element by the radioactive decay of U and Th. Considering the Paleoproterozoic age of the carbonaceous schists, Pb could be readily accumulated in a concentration sufficient for its analysis on a microprobe, which provides

**Table 5.** Mineral associations of silicate (rock-forming) and accessory REE-bearing minerals

Sample	Mineral association	REE-bearing accessory mineral
Garnet zone		
8617/300	<i>Qtz + Bt + Pl + Chl</i>	<i>Bst + Ap</i>
8617/404	<i>Qtz + Pl + Kfs + Bt + Chl</i>	<i>Bst + Ap</i>
8062/380	<i>Qtz + Bt + Ms + Chl</i>	<i>Mnz + Ap + Zrn</i>
820/318	<i>Qtz + Bt + Chl + Pl + Ms + Gph</i>	<i>Bst + Mnz</i>
542-c/173	<i>Qtz + Bt + Pl + Chl + Gph</i>	<i>Bst + Ap</i>
8305/1	<i>Qtz + Chl + Bt + Ms</i>	<i>Bst</i>
8200/209	<i>Qtz + Ms + Chl + Bt</i>	<i>Bst + Mnz</i>
548-c/4	<i>Qtz + Chl + Pl + Kfs</i>	<i>Bst + Mnz + Xen + Ap</i>
7522/308	<i>Qtz + Bt + Czo + Pl + Kfs</i>	<i>Bst + Syn</i>
7004/264	<i>Qtz + Bt + Pl + Kfs + Gph</i>	<i>Bst + Mnz</i>
8186/400	<i>Qtz + Pl + Ms + Chl + Bt + Gph</i>	<i>Mnz</i>
8731/402	<i>Qtz + Pl + Ms + Chl + Bt</i>	<i>Bst + Mnz</i>
8601/425	<i>Qtz + Pl + Kfs + Chl + Bt + Tur</i>	<i>Mnz + Ap</i>
Staurolite zone		
8712/4	<i>Qtz + Pl + Bt + Chl + Grt + St</i>	<i>Mnz + Aln + Ap</i>
8010/287	<i>Qtz + Pl + St + Ms + Bt</i>	<i>Mnz + Aln + Ap</i>
8283/8	<i>Qtz + Ms + Bt + Chl + Pl + St</i>	<i>Mnz + Ap + Xen</i>
809/6	<i>Qtz + Pl + Chl + Bt + St</i>	<i>Mnz</i>
Staurolite–sillimanite zone		
8358/1	<i>Qtz + Pl + Ms + Bt + St + Sil</i>	<i>Mnz + Xen</i>
8053/275	<i>Qtz + Bt + Ms + Pl + St + Sil</i>	<i>Mnz + Xen + Ap</i>
8312/1	<i>Qtz + St + Bt + Pl + Ms + Sil</i>	<i>Mnz + Xen + Ap</i>
8384/430	<i>Qtz + Pl + Kfs + Bt + Ms + St + Sil + Gph</i>	<i>Mnz + Ap</i>
Muscovite–sillimanite zone		
8240/352	<i>Qtz + Bt + Pl + Ms + Sil</i>	<i>Mnz</i>
8371/488	<i>Qtz + Bt + Ms + Pl + Sil</i>	<i>Mnz</i>
8703/322	<i>Qtz + Pl + Bt + Ms + Sil</i>	<i>Mnz</i>
7103/503	<i>Qtz + Bt + Ms + Pl + Sil</i>	<i>Mnz</i>
8354/378	<i>Qtz + Bt + Ms + Pl + Sil</i>	<i>Mnz + Ap</i>
Sillimanite–potassic feldspar–cordierite zone		
4n/170	<i>Qtz + Pl + Bt + Sil + Crd + Gph</i>	<i>Mnz + Zrn</i>
1n/119	<i>Qtz + Pl + Bt + Crd + Sil + Gph</i>	<i>Mnz</i>
242-a/310	<i>Qtz + Pl + Bt + Crd + Grt + Sil</i>	<i>Mnz</i>

a basis for CHIME chemical dating of monazite (Suzuki et al., 1994).

**Bastnaesite**, a F-carbonate of REE, belongs to the parisite group and has the empirical formula  $(\text{Ce}, \text{La})(\text{CO}_3)\text{F}$ ; this mineral is widespread only in the garnet zone and has never been found in higher temperature zones. The mineral was detected in two morphological types. It occurs in the matrix as elongated prismatic crystals from 10 to 100  $\mu\text{m}$  long (Figs. 5e, 8a, 8b), and its large grains are sometimes zonal (Fig. 8b). The other morphological type comprises small (10–

20  $\mu\text{m}$ ) acicular crystals and rosettes of this mineral that replace chlorite (Figs. 8d, 8e), biotite (5d), and plagioclase (Fig. 8c).

Both morphological types of bastnaesite are similar in composition and display the predominance of Ce (25–32 wt %  $\text{Ce}_2\text{O}_3$ ), whose concentrations are roughly twice higher than those of La and Nd (8–16 wt %  $\text{La}_2\text{O}_3$  and  $\text{Nd}_2\text{O}_3$  each) (Table 8). Other REE contained in appreciable concentrations in the mineral are Pr (2–4 wt %  $\text{Pr}_2\text{O}_3$ ) and Y (up to 5.3 wt %  $\text{Y}_2\text{O}_3$ ). The Th concentrations in the bastnaesite is no higher than 1 wt %  $\text{ThO}_2$ ,

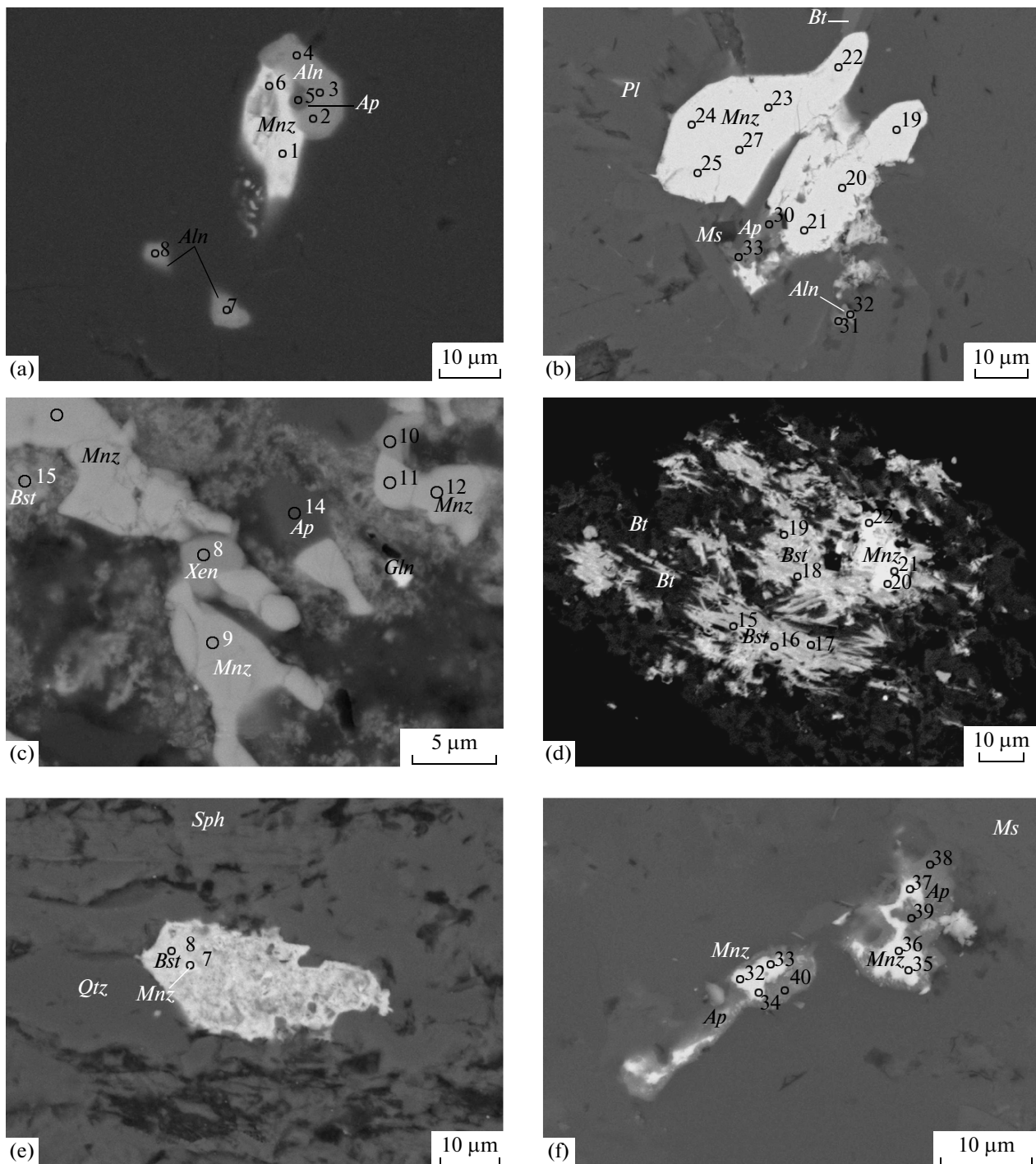


**Fig. 5.** Relations between REE-bearing minerals in low- and medium-temperature metapelites of the Vorontsovskaya Group. (a) Allanite in contact with monazite and apatite (staurolite zone, sample 8712/4); (b) tiny allanite relics in association with monazite and apatite (staurolite zone, sample 8010/287); (c) monazite in association with bastnaesite, xenotime, and apatite (garnet zone, sample 548-c/4); (d) bastnaesite replacing biotite and monazite replacing bastnaesite (garnet zone, sample 8200/209); (e) tiny monazite inclusions in bastnaesite (garnet zone, sample 7004/264); (f) monazite inclusions in apatite (garnet zone, sample 8062/380). The numbers of analytical spots in this and other figures correspond to the numbers of microprobe analyses in Tables 6–10.

and this element was not detected in some bastnaesite grains. The Ca concentrations broadly vary, from 0.7 to almost 9 wt % CaO. Similar REE proportions were detected in the allanite and bastnaesite.

The only exception is bastnaesite in sample 548-c/4, in which this mineral is in close association with monazite (Fig. 8f). Unfortunately, the small size of the grains ( $<10 \mu\text{m}$ ) allowed us to analyze only one of

**Table 6.** Composition of allanite in metapelites of the Vorontsovskaya Group

Component	Sample 8712/4					Sample 8010/287	
	2	3	4	7	8	31	32
P <sub>2</sub> O <sub>5</sub>	0.52	0.10	0.89	—	0.33	—	3.19
SiO <sub>2</sub>	31.63	30.98	31.04	32.21	31.19	36.19	34.44
ThO <sub>2</sub>	1.69	2.26	1.60	0.34	1.57	—	—
Al <sub>2</sub> O <sub>3</sub>	16.58	17.64	16.83	18.40	17.83	20.02	21.14
La <sub>2</sub> O <sub>3</sub>	5.53	4.62	5.38	5.09	5.71	2.16	2.96
Ce <sub>2</sub> O <sub>3</sub>	12.50	12.30	13.18	11.53	12.49	5.81	8.07
Pr <sub>2</sub> O <sub>3</sub>	0.84	0.72	0.88	0.73	0.54	0.44	0.52
Nd <sub>2</sub> O <sub>3</sub>	4.84	3.83	4.14	4.28	4.36	2.84	3.42
FeO	11.37	11.55	11.28	12.09	11.64	8.70	8.88
MnO	0.59	0.49	0.44	0.43	0.61	—	—
MgO	0.49	0.63	0.58	0.36	0.62	—	0.56
CaO	10.72	11.30	10.47	11.46	10.90	17.40	11.27
Na <sub>2</sub> O	0.21	0.19	0.01	0.42	—	2.30	1.71
Total	97.51	96.61	96.72	97.34	97.79	95.86	96.16
P	0.04	0.01	0.07	—	0.03	—	0.24
Si	3.04	2.96	3.01	3.00	2.97	3.07	3.02
Th	0.04	0.05	0.04	0.01	0.03	—	—
Al	1.88	1.99	1.92	2.02	2.00	2.00	2.19
La	0.20	0.16	0.19	0.17	0.20	0.07	0.10
Ce	0.44	0.43	0.47	0.39	0.43	0.18	0.26
Pr	0.03	0.03	0.03	0.02	0.02	0.01	0.02
Nd	0.17	0.13	0.14	0.14	0.15	0.09	0.11
Fe	0.91	0.92	0.91	0.94	0.93	0.62	0.65
Mn	0.05	0.04	0.04	0.03	0.05	—	—
Mg	0.07	0.09	0.08	0.05	0.09	—	0.07
Ca	1.10	1.16	1.09	1.14	1.11	1.58	1.06
Na	0.04	0.04	—	0.08	—	0.38	0.29
ΣREE	0.84	0.75	0.83	0.55	0.60	0.28	0.39

Note: Cation proportions were calculated by normalizing to the total of cations (8). Here and in other tables, dashes mean concentrations of elements below the detection limit. The numbers of analyses correspond to analytical spot numbers in Figs. 5–8. Here and in Tables 7–10, oxides are given in wt % and elements are in ppm.

them (Fig. 8e, analytical spot 16) without interference of other phases in the EDS analyses. In this bastnaesite analysis, REE are dominated by Pr (31.8 wt % Pr<sub>2</sub>O<sub>3</sub>), Yb (12.24 wt % Yb<sub>2</sub>O<sub>3</sub>), and Ce (11.45 wt % Ce<sub>2</sub>O<sub>3</sub>) (Table 8). The mineral contains minor amounts of La (3.55 wt % La<sub>2</sub>O<sub>3</sub>) and Nd (1.73 wt % Nd<sub>2</sub>O<sub>3</sub>). Another bastnaesite grain (Fig. 5c, spot 15) has a similar composition but additionally contains much P and Si (Table 8), which is likely explained by the involvement of quartz and monazite in the analytical spot of the microprobe beam. This Pr-rich bastnaesite is also rich in Mn (approximately 4 wt % MnO). It is pertinent to mention that no bastnaesite of such composi-

tion has been found so far, although Ce-, La-, and Y-bearing bastnaesite is known.

The bastnaesite was found in association with **synchysite** Ca(Ce,La,Nd)(CO<sub>3</sub>)<sub>2</sub>F, a calcic end member of bastnaesite–synchysite isomorphic series (Fig. 8b). The synchysite differs from bastnaesite in bearing higher concentrations of Ca (10–16 wt % CaO) and, correspondingly, lower concentrations of Ce (23–27 wt % Ce<sub>2</sub>O<sub>3</sub>) and La (12.7–15.9 wt % La<sub>2</sub>O<sub>3</sub>) (Table 8). Some synchysite crystals are zonal (Table 8b, Table 8) and have paler cores of bastnaesite and margins (darker) of synchysite.

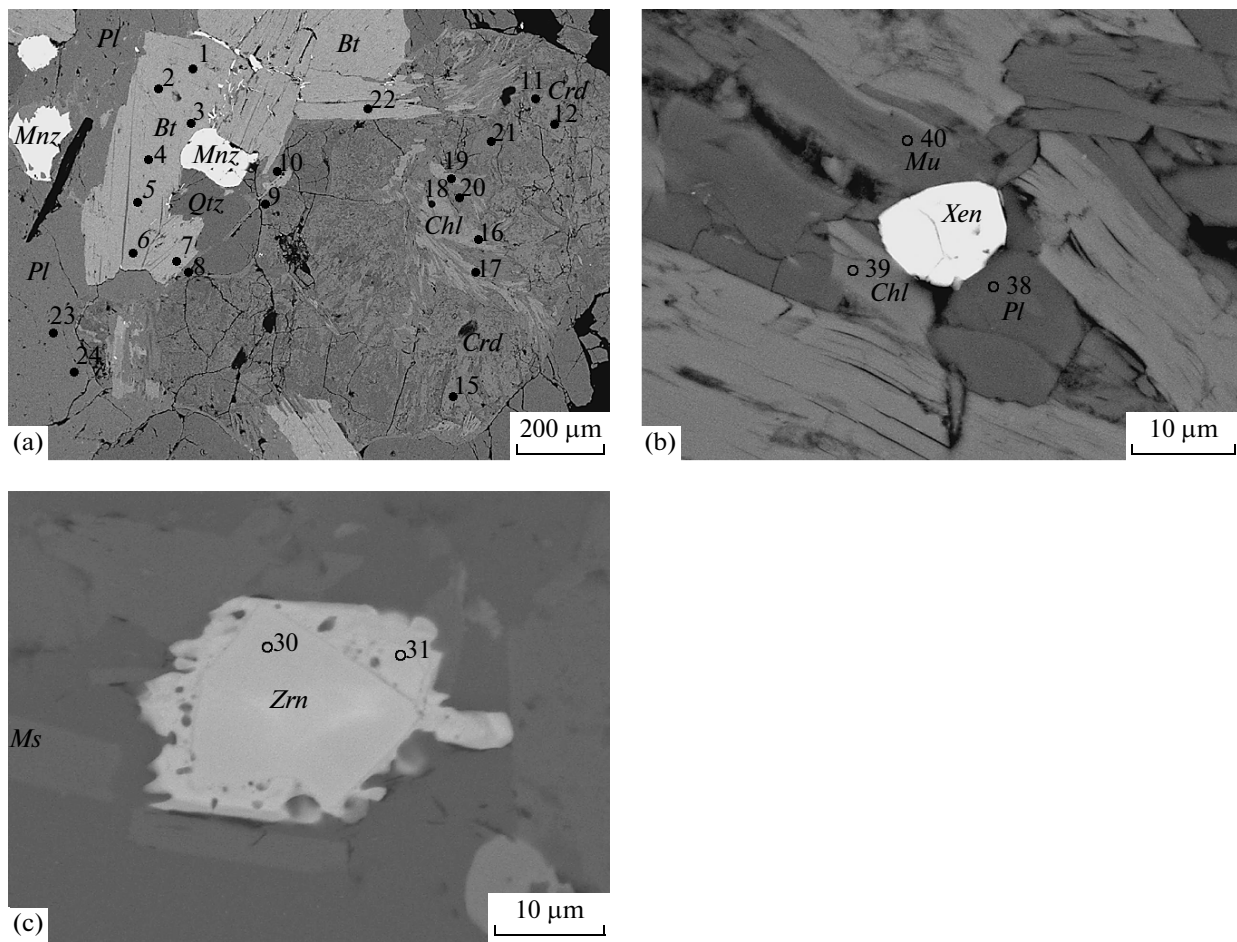


**Fig. 6.** REE-bearing minerals from metapelites of the medium- and high-temperature zones of the Vorontsovskaya Group, Voronezh Crystalline Massif. (a) Large monazite grain in graphite gneiss (sample 4n/170, sillimanite–potassic feldspar–cordierite zone); (b) xenotime grain in a silicate matrix of crystalline schist (sample 8053/275, staurolite–sillimanite zone); (c) REE-bearing zircon (sample 8062/380, garnet zone).

**Apatite**  $(\text{Ca}, \text{REE})_5[\text{PO}_4]_3(\text{F}, \text{OH})$  was found in metasedimentary rocks of the Vorontsovskaya Group as single grains in the matrix and in reaction textures, together with monazite, allanite, and bastnaesite, in the garnet and staurolite zones (Figs. 5a–5c, 5f). The apatite sometimes contains REE. For example, small apatite grains (approximately 5  $\mu\text{m}$ ) in association with monazite and allanite in sample 8010/287 contain close to 4.4 wt % REE, with the maximum concentration of these elements detected in sample 8712/4: 13.5 wt % (Fig. 5a, Table 9). Apatite with monazite inclusions is depleted in REE (about 1 wt %) but is richer in Th (1.7–3.9 wt %  $\text{ThO}_2$ ) (Fig. 5f, Table 9), whereas no REE were detected in the apatite with monazite lamellas. Single apatite grains in the matrix usually contain no REE. All of the apatite grains are F-apatite.

**Xenotime**  $[\text{YPO}_4]$  is an HREE phosphate. It was most often found in staurolite-bearing assemblages, together with monazite, as single grains 10–40  $\mu\text{m}$

across of equant or elongated shape (Figs. 5c, 6b). The xenotime bears low concentrations of Si (1.5–2.5 wt %  $\text{SiO}_2$ ), which isomorphically substitutes P and shows a deficit in Y (approximately 0.8 f.u.), an element substituted for HREE (approximately 12 wt % in total) (Table 10). The mineral also contains Ca (up to 3 wt %  $\text{CaO}$ ), U (up to 1.5 wt %  $\text{UO}_3$ ), Th (up to 1.5 wt %  $\text{ThO}_2$ ), and Pb (up to 1.5 wt %  $\text{PbO}$ ). Small (no larger than 5  $\mu\text{m}$ ) xenotime grains in contact with monazite contain much LREE (2–3 wt %  $\text{La}_2\text{O}_3$  and 5–9 wt %  $\text{Ce}_2\text{O}_3$ ). The xenotime was formed during the partial decomposition of garnet in the staurolite zone, because garnet is the only rock-forming silicate able to concentrate Y.

The silicate matrix of sample 8062/380 contains zircon with 0.3–0.8 wt %  $\text{Ce}_2\text{O}_3$  and 0.5–1 wt %  $\text{Pr}_2\text{O}_3$  (Fig. 6c).

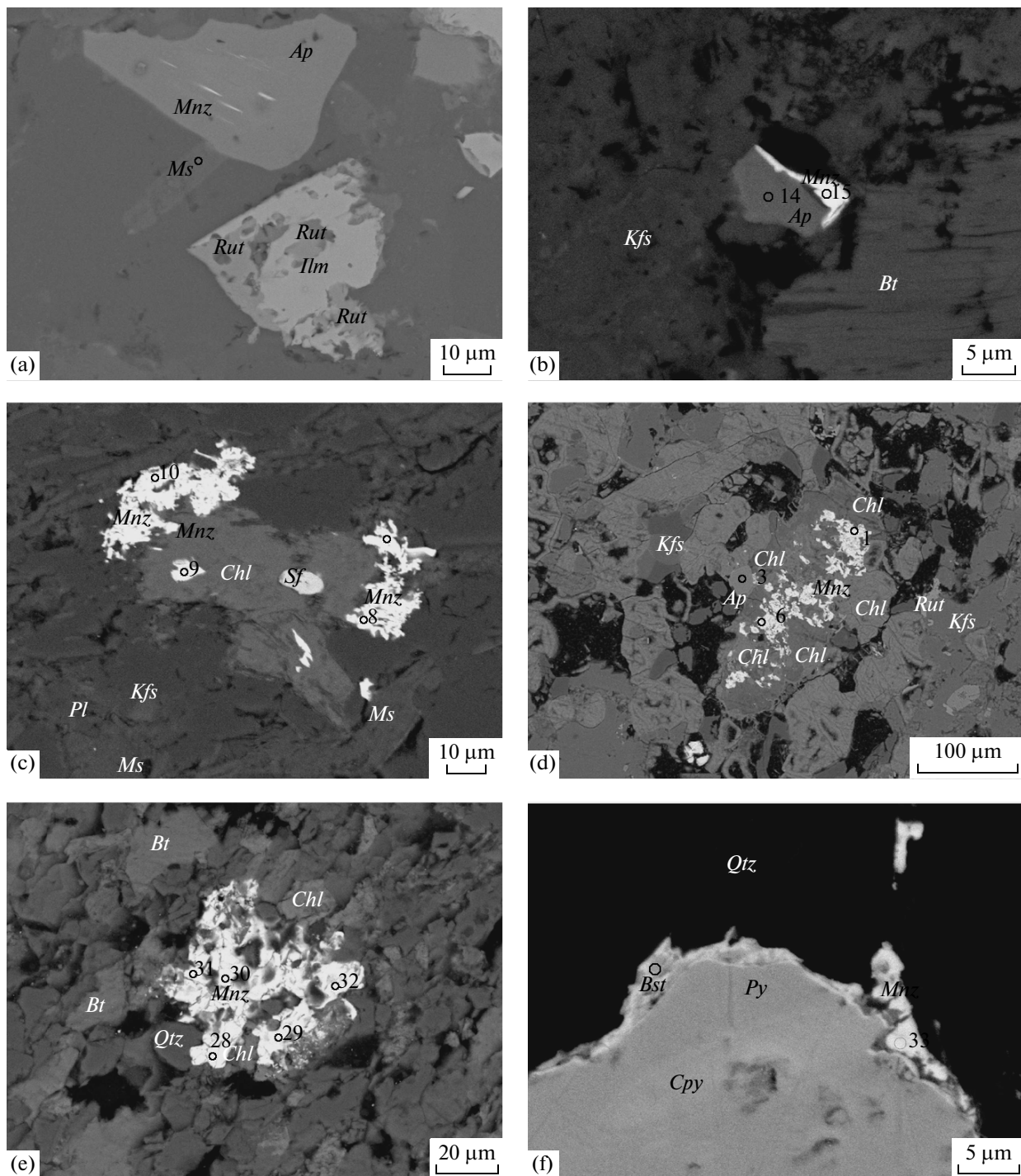


**Fig. 7.** Reaction textures of REE-bearing minerals in metapelites of the Vorontsovskaya Group, Voronezh Crystalline Massif. (a) Thin monazite lamellas oriented in cleavage planes in apatite (garnet zone, sample 8062/380); (b) monazite rim around apatite (staurolite zone, sample 8384/430); (c) monazite growing along margins of a chlorite grain (garnet zone, sample 8186/400); (d) monazite developing in the core of a large chlorite grain (garnet zone, sample 8601/425); (e) chlorite replaced by monazite (garnet zone, sample 548-c/4); (f) monazite and bastnaesite rims around pyrite (garnet zone, sample 8731/402).

### INTERPRETATIONS OF MINERAL EQUILIBRIA

As was mentioned above, bastnaesite occurs only in the garnet zone, in which it is spread fairly widely

(Table 5). This testifies that the mineral was formed during the metamorphism of rocks of the Vorontsovskaya Group but was not an overprinted (epigenetic) phase, because otherwise bastnaesite should

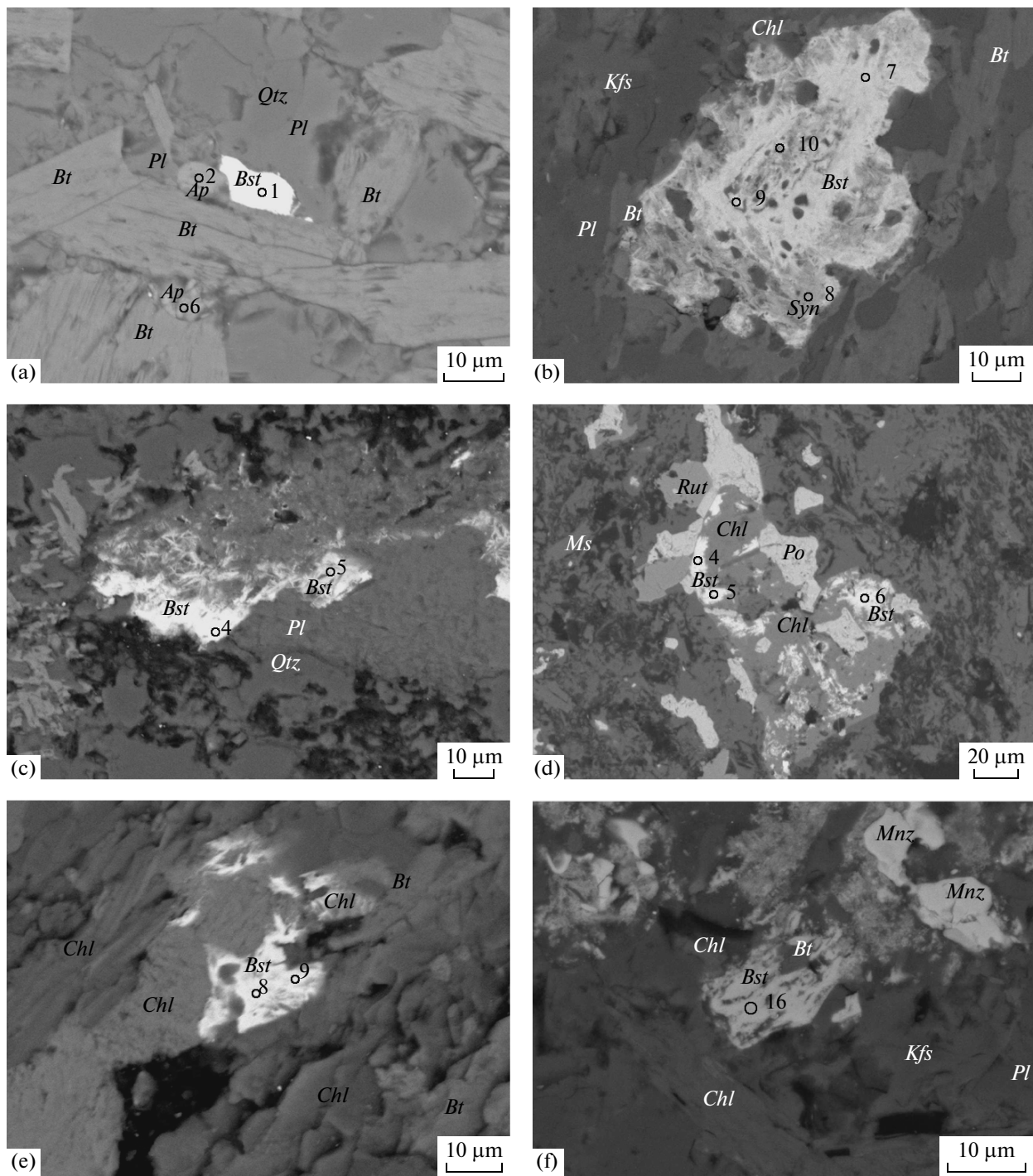


**Fig. 8.** Bastnaesite relations with other minerals in metapelites of the Vorontsovskaya Group, Voronezh Crystalline Massif. (a) Bastnaesite in contact with apatite in the rock matrix (sample 8617/404); (b) large zonal bastnaesite grain with an outer synchysite zone (sample 7522/308); (c) bastnaesite replacing plagioclase (sample 7004/264); (d) bastnaesite inclusion in chlorite (sample 8305/1); (e) chlorite replaced by bastnaesite (sample 820/318); (f) “Pr”-bastnaesite in association with monazite, xenotime, and apatite (sample 548-c/4).

have also occurred in other (higher temperature) metamorphic zones. Bastnaesite commonly exhibits reaction relations with monazite and phyllosilicates (biotite and chlorite). The mineral was formed at the

recrystallization of detrital bastnaesite or monazite during greenschist-facies metamorphism, although other mechanisms were also possible. Bastnaesite could have replaced chlorite (Figs. 8d, 8e, 8f) or, more

**Table 7.** Composition and cation proportions in the formula of monazite from metapelites of the Vorontsovskaya Group

Component	809/6	7004/264	548-c/4	820/318	8062/380	8712/4	8200/209	8010/287	23
	3	7	12	32	34	35	1	6	
UO <sub>3</sub>	0.57	0.11	0.66	0.13	0.29	0.63	0.01	0.60	0.42
P <sub>2</sub> O <sub>5</sub>	30.91	27.91	29.85	31.03	30.54	30.42	28.25	24.92	30.16
SiO <sub>2</sub>	0.37	1.39	1.52	0.48	1.60	3.39	1.30	6.30	0.75
ThO <sub>2</sub>	4.05	4.28	4.10	3.92	3.04	5.04	3.05	3.15	2.19
Al <sub>2</sub> O <sub>3</sub>	0.26	0.25	0.52	0.54	—	—	0.32	1.10	—
La <sub>2</sub> O <sub>3</sub>	14.12	14.05	12.28	14.28	11.16	11.12	14.93	14.82	13.90
Ce <sub>2</sub> O <sub>3</sub>	31.88	30.82	28.79	29.38	27.54	26.34	33.00	32.17	30.29
Pr <sub>2</sub> O <sub>3</sub>	3.15	3.57	3.19	2.03	3.14	3.21	2.05	1.58	2.45
Nd <sub>2</sub> O <sub>3</sub>	12.03	12.30	11.35	11.11	11.52	10.36	11.17	10.36	11.12
Sm <sub>2</sub> O <sub>3</sub>	—	1.73	1.08	1.73	1.95	1.54	0.26	1.26	2.22
Gd <sub>2</sub> O <sub>3</sub>	—	0.56	1.32	1.48	1.61	0.78	0.74	1.00	1.84
Eu <sub>2</sub> O <sub>3</sub>	—	—	—	1.19	0.73	0.58	0.03	—	0.91
CaO	1.00	1.48	1.35	0.87	4.60	5.85	0.57	1.07	0.80
FeO	—	0.01	0.08	—	0.28	0.40	—	0.78	0.38
PhO	0.35	0.09	1.01	0.10	0.24	0.27	0.41	0.32	0.82
F	0.66	0.49	0.88	0.74	—	—	—	—	0.37
Total	99.35	99.04	97.98	99.01	98.24	99.93	96.09	99.44	96.57
U	—	—	0.01	—	—	—	—	—	—
P	1.02	0.93	0.98	1.02	0.95	0.91	0.96	0.79	1.00
Si	0.01	0.05	0.06	0.02	0.06	0.12	0.05	0.23	—
Th	0.04	0.04	0.04	0.03	0.03	0.04	0.03	0.03	0.02
Al	0.01	0.01	0.02	0.02	—	—	0.02	0.05	—
La	0.20	0.20	0.18	0.20	0.15	0.14	0.22	0.20	0.21
Ce	0.45	0.44	0.41	0.42	0.37	0.34	0.49	0.44	0.45
Pr	0.04	0.05	0.05	0.03	0.04	0.04	0.03	0.02	0.04
Nd	0.17	0.17	0.16	0.15	0.15	0.13	0.16	0.14	0.16
Sm	—	0.02	0.01	0.02	0.02	0.02	—	0.02	0.03
Gd	—	0.01	0.02	0.02	0.02	0.01	0.01	0.01	0.02
Eu	—	—	—	0.02	0.01	0.01	—	0.01	0.01
Ca	0.04	0.06	0.06	0.04	0.18	0.22	0.02	0.04	0.03
Fe	—	—	—	—	0.01	0.01	—	0.01	—
Pb	—	—	0.01	—	—	—	0.01	—	0.01
ΣREE	0.86	0.89	0.83	0.86	0.76	0.69	0.91	0.83	0.92

Table 7. (Contd.)

Component	8283/8	8358/1	8053/275	8312/1	8240/352	8703/322	4n/170	In/119
	25	10	11	15	9	21	47	7
UO <sub>3</sub>	0.61	—	1.19	0.36	0.95	0.68	0.76	0.04
P <sub>2</sub> O <sub>5</sub>	29.36	30.12	27.23	29.27	31.10	28.11	29.67	28.16
SiO <sub>2</sub>	0.44	0.89	0.67	0.85	0.35	0.54	0.33	0.70
ThO <sub>2</sub>	2.86	3.70	2.05	4.62	2.44	2.08	2.27	2.52
Al <sub>2</sub> O <sub>3</sub>	—	—	—	—	—	—	—	—
La <sub>2</sub> O <sub>3</sub>	13.38	14.18	12.78	13.10	11.90	13.58	12.81	14.66
Ce <sub>2</sub> O <sub>3</sub>	30.55	30.78	29.30	29.42	30.88	33.90	32.34	31.19
Pr <sub>2</sub> O <sub>3</sub>	3.49	3.16	3.63	3.08	3.54	3.92	4.15	4.74
Nd <sub>2</sub> O <sub>3</sub>	13.61	11.09	13.27	12.19	13.20	13.45	12.37	13.26
Sm <sub>2</sub> O <sub>3</sub>	1.33	1.75	3.52	3.59	1.31	0.90	1.78	1.69
Gd <sub>2</sub> O <sub>3</sub>	1.05	1.50	1.76	0.59	2.24	0.52	1.80	1.88
Eu <sub>2</sub> O <sub>3</sub>	0.40	0.15	1.16	0.88	0.21	—	0.32	0.06
CaO	0.72	0.89	0.67	1.10	0.75	0.64	0.79	0.58
FeO	0.09	—	0.12	0.46	0.17	—	—	—
PbO	0.65	0.20	0.47	0.20	0.73	0.48	—	—
Total	98.54	98.41	97.82	99.71	99.77	98.8	99.39	99.48
U	0.01	—	0.01	—	0.01	0.01	—	0.01
P	0.99	1.00	0.94	0.97	1.02	0.95	0.99	1.02
Si	0.02	0.03	0.03	0.03	0.01	0.02	0.03	0.03
Th	0.03	0.03	0.02	0.04	0.02	0.02	0.02	0.02
Al	—	—	—	—	—	—	—	—
La	0.20	0.21	0.19	0.19	0.17	0.20	0.19	0.22
Ce	0.44	0.44	0.44	0.42	0.44	0.50	0.47	0.45
Pr	0.05	0.05	0.05	0.04	0.05	0.06	0.06	0.07
Nd	0.19	0.16	0.19	0.17	0.18	0.19	0.17	0.19
Sm	0.02	0.02	0.05	0.05	0.02	0.01	0.02	0.01
Gd	0.01	0.02	0.02	0.01	0.03	0.01	0.02	0.01
Eu	0.01	—	0.02	0.01	—	—	—	—
Ca	0.03	0.04	0.03	0.05	0.03	0.03	0.02	0.01
Fe	—	—	—	0.02	0.01	—	—	—
Pb	0.01	—	0.01	—	0.01	0.01	—	0.01
ΣREE	0.92	0.90	0.96	0.89	0.89	0.97	0.93	0.97

Note: Crystal chemical coefficients were calculated by normalizing to 2 cations.

**Table 8.** Composition and cation proportions in the formula of bastnaesite and synchysite from metapelites of the Vorontsovskaya Group

Com- ponent	542- c/173				7004/264				548-c/4				820/318				86/7/300				8617/ 404				8305/1				8731/ 402			
	Bst	Bst	Syn	Bst	Bst	Bst	Bst	Bst	Bst	Bst	Bst	Bst	Bst	Bst	Bst	Bst	Bst	Bst	Bst	Bst	Bst	Bst	Bst	Bst	Bst	Bst	Bst	Bst	Bst	Bst		
UO <sub>3</sub>	0.24	—	0.04	—	0.09	0.08	—	0.28	0.12	—	0.54	0.02	0.69	0.21	—	0.02	0.55	0.57	—	0.23	—	—	0.11	0.09	—	—	—	—	—	1.21		
SO <sub>3</sub>	0.15	1.29	—	0.12	0.46	0.23	0.26	—	—	—	—	—	—	—	—	—	—	—	—	—	—	—	—	—	—	—	—	—	—			
P <sub>2</sub> O <sub>5</sub>	0.07	—	0.02	0.09	8.64	2.42	—	—	0.38	—	0.20	0.05	0.04	0.23	0.23	0.07	—	—	—	—	—	—	—	—	—	—	—	—	—			
SiO <sub>2</sub>	0.61	0.14	1.47	1.00	4.52	0.82	1.71	0.66	0.96	4.46	2.42	3.88	1.78	1.54	2.90	0.37	5.49	0.58	1.93	0.58	—	—	—	—	—	—	—	—	3.11			
ThO <sub>2</sub>	0.57	1.15	0.50	0.64	2.06	0.72	0.68	—	0.50	—	—	0.47	0.57	1.11	1.91	0.51	—	0.41	0.83	0.83	0.41	0.83	0.83	0.83	0.83	0.83	0.83	0.83	0.55			
Al <sub>2</sub> O <sub>3</sub>	0.16	0.57	0.38	0.19	1.29	0.70	0.58	0.35	0.85	2.12	1.86	3.15	0.96	0.64	1.05	0.64	3.24	0.23	0.31	0.31	—	—	—	—	—	—	—	—	2.46			
Y <sub>2</sub> O <sub>3</sub>	0.58	0.35	1.49	0.32	2.11	0.22	—	0.32	1.89	2.11	3.11	2.21	5.26	0.56	0.48	0.25	3.09	1.73	2.87	2.87	—	—	—	—	—	—	—	—	2.27			
La <sub>2</sub> O <sub>3</sub>	14.29	16.21	8.49	16.20	2.94	3.55	14.94	15.76	9.22	8.80	12.20	10.54	13.71	14.98	14.85	15.97	10.20	13.50	5.62	5.62	—	—	—	—	—	—	—	—	13.20			
Ce <sub>2</sub> O <sub>3</sub>	32.03	33.01	24.47	31.09	10.06	11.45	27.80	31.46	26.21	23.60	27.87	24.45	31.99	30.44	26.38	31.44	23.38	31.24	16.54	16.54	—	—	—	—	—	—	—	—	25.43			
Pr <sub>2</sub> O <sub>3</sub>	2.44	2.95	3.40	2.92	25.32	31.79	2.08	3.05	2.22	3.10	2.89	1.61	1.88	3.92	4.04	3.33	1.73	2.05	1.65	1.65	—	—	—	—	—	—	—	—	1.74			
Nd <sub>2</sub> O <sub>3</sub>	11.37	11.68	7.97	12.20	1.51	1.73	10.96	11.50	10.64	8.39	11.17	9.18	10.97	10.80	10.87	10.26	8.93	10.73	6.78	6.78	—	—	—	—	—	—	—	—	10.01			
Yb <sub>2</sub> O <sub>3</sub>	—	0.43	—	11.00	12.24	—	1.08	—	—	—	—	—	—	—	—	—	—	—	—	—	—	—	—	—	—	—	—	—	—			
CaO	3.58	3.76	16.38	4.10	0.73	0.75	2.18	3.66	6.66	8.65	10.23	12.70	11.48	5.01	4.21	5.77	14.74	3.93	13.76	13.76	—	—	—	—	—	—	—	—	3.86			
MnO	0.10	0.16	—	0.13	4.10	4.09	0.21	0.16	—	—	—	0.15	0.46	—	—	—	—	—	0.15	0.15	—	—	—	—	—	—	—	0.05				
FeO	0.42	—	1.30	0.35	—	0.18	4.91	0.26	0.86	4.55	0.06	1.07	—	1.41	3.64	1.51	1.71	—	—	—	—	—	—	—	—	—	3.59					
PbO	0.25	—	0.47	—	—	0.03	—	—	0.16	—	0.03	—	0.69	0.57	0.39	0.39	—	—	0.15	0.15	—	—	—	—	—	—	—	0.39				
F	3.72	8.53	6.62	7.42	6.95	9.29	5.41	5.33	5.83	5.86	6.18	5.79	7.20	5.31	6.27	5.95	8.49	8.49	9.89	9.89	5.68	5.68	—	—	—	—	—	—	—	8.99		
Total	70.58	80.23	73.00	76.77	81.78	80.29	71.72	73.87	66.34	71.8	78.73	75.15	86.53	77.00	77.86	76.48	82.19	76.45	56.75	56.75	77.20	—	—	—	—	—	—	—	—			
U	—	—	—	—	—	—	—	—	—	—	—	—	—	—	—	—	—	—	—	—	—	—	—	—	—	—	—	—	—	0.01		
S	—	0.03	—	—	—	0.01	0.01	0.01	0.01	—	—	—	—	—	—	—	—	—	—	—	—	—	—	—	—	—	—	—	—			
P	—	—	—	—	—	0.03	0.12	0.03	0.06	0.02	0.03	0.12	0.06	0.10	0.04	0.05	0.09	0.01	0.01	0.01	—	—	—	—	—	—	—	—	—	—		
Si	0.02	—	0.08	—	—	0.01	—	—	—	—	—	—	—	—	—	—	—	—	—	—	—	—	—	—	—	—	—	—	—	0.09		
Th	—	0.01	—	0.01	—	0.01	0.01	0.01	0.01	—	—	—	—	—	—	—	—	—	—	—	—	—	—	—	—	—	—	—	—			
Al	0.01	0.02	0.02	0.01	0.04	0.03	0.02	0.01	0.03	0.07	0.06	0.09	0.03	0.02	0.04	0.02	0.04	0.01	0.01	0.01	—	—	—	—	—	—	—	—	0.09			
Y	0.01	0.01	0.04	0.01	0.03	—	—	0.01	0.03	0.03	0.04	0.03	0.07	0.01	0.01	—	—	0.04	0.03	0.10	0.10	0.04	0.10	0.04	0.10	0.04	0.15					
La	0.19	0.20	0.17	0.20	0.03	0.04	0.19	0.20	0.12	0.09	0.12	0.10	0.13	0.17	0.16	0.19	0.08	0.18	0.14	0.14	0.15	0.15	0.15	0.15	0.15	0.15	0.15					
Ce	0.42	0.41	0.47	0.39	0.10	0.14	0.34	0.40	0.33	0.23	0.27	0.22	0.30	0.35	0.29	0.37	0.19	0.42	0.40	0.40	0.40	0.40	0.40	0.40	0.40	0.40	0.28					
Pr	0.03	0.04	0.07	0.04	0.25	0.39	0.03	0.04	0.03	0.03	0.03	0.02	0.04	0.04	0.04	0.04	0.04	0.04	0.04	0.04	0.04	0.04	0.04	0.04	0.04	0.04	0.04	0.02				
Nd	0.15	0.14	0.15	0.15	0.01	0.02	0.13	0.14	0.13	0.08	0.11	0.08	0.10	0.12	0.12	0.12	0.07	0.14	0.16	0.16	0.16	0.16	0.16	0.16	0.16	0.16	0.11					
Yb	—	—	—	—	—	0.09	0.12	—	0.01	—	—	—	—	—	—	—	—	—	—	—	—	—	—	—	—	—	—	—	—			
Ca	0.14	0.14	0.93	0.15	0.02	0.03	0.08	0.14	0.25	0.29	0.34	0.31	0.17	0.13	0.20	0.35	0.15	0.98	0.98	0.98	0.98	0.98	0.98	0.98	0.98	0.98	0.12					
Mn	—	—	—	—	—	0.09	0.12	0.01	—	—	—	—	—	—	—	—	—	—	—	—	—	—	—	—	—	—	—	—	—			
Fe	0.01	—	—	0.06	0.01	—	0.01	0.04	0.02	0.10	—	—	0.04	0.09	0.04	0.04	0.04	0.03	—	—	—	—	—	—	—	—	—	0.09				
Pb	—	—	0.01	—	—	—	—	—	—	—	—	—	—	—	—	—	—	—	—	—	—	—	—	—	—	—	—	—	—	—		
F	0.30	0.80	0.85	0.65	0.74	0.85	0.43	0.45	0.39	0.46	0.60	0.50	0.50	0.50	0.50	0.50	0.50	0.50	0.50	0.50	0.50	0.50	0.50	0.50	0.50	0.50	0.50	0.74				

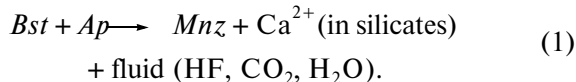
Note: Cation proportions of bastnaesite and synchysite were calculated by normalizing to a total of cations of 1 and 2, respectively.

**Table 9.** Composition of apatite from metapelites of the Vorontsovskaya Group

Com- ponent	542- c/173	542-c	8601/ 425	8062/380						8712/4	8010/287			8283/8	
	2	14	3	22	23	24	38	39	40	5	10	30	33	12	14
F	4.25	6.62	3.39	2.77	4.84	2.96	4.34	5.11	4.32	3.03	3.65	5.01	3.87	4.05	3.84
P <sub>2</sub> O <sub>5</sub>	41.04	38.40	41.33	42.23	40.47	39.55	32.12	31.92	34.83	36.42	40.75	39.37	34.90	39.74	39.21
CaO	53.29	49.41	53.45	54.25	53.03	52.20	41.33	37.63	42.76	42.29	52.26	49.62	43.86	53.52	52.98
SiO <sub>2</sub>	0.61	1.52	0.18	0.20	0.48	1.72	9.44	20.61	9.21	2.09	0.69	0.76	6.58	0.57	0.81
FeO	0.31	0.62	0.44	—	0.07	0.10	2.10	0.50	1.17	0.42	0.41	—	0.35	0.28	0.48
Al <sub>2</sub> O <sub>3</sub>	0.28	0.95	0.04	—	—	—	3.13	0.05	0.42	0.94	—	0.40	4.48	0.10	0.50
SO <sub>3</sub>	0.02	0.09	0.07	—	—	—	0.79	—	0.23	0.18	—	0.20	0.24	—	0.14
La <sub>2</sub> O <sub>3</sub>	—	—	—	—	—	—	0.42	0.09	0.15	3.46	—	1.18	0.98	0.15	0.29
Ce <sub>2</sub> O <sub>3</sub>	0.12	1.93	0.57	—	—	—	0.92	0.72	0.64	6.77	—	2.29	2.01	—	0.43
Nd <sub>2</sub> O <sub>3</sub>	—	—	—	—	—	—	—	—	—	2.80	—	0.90	1.43	—	0.02
Dy <sub>2</sub> O <sub>3</sub>	—	—	—	—	—	—	—	—	—	0.52	—	—	—	0.77	0.14
ThO <sub>2</sub>	—	—	—	0.22	0.49	0.42	2.73	1.70	3.91	0.82	—	0.22	—	0.02	0.47
Total	99.92	99.54	99.47	99.67	99.38	96.95	97.32	98.33	97.64	99.74	97.76	99.95	98.7	99.2	99.31

rarely, biotite (Fig. 5d) and plagioclase (Fig. 8c) and form acicular crystals and their rosettes at the partial decomposition of silicates bearing REE in concentrations from a few dozen to a few hundred ppm (Lanziotti and Hanson, 1996; Kohn and Malloy, 2004; Corrie and Kohn, 2008). Such textures were interpreted as produced by bastnaesite crystallization due to the partial decomposition of LREE-bearing (up to 2.5 wt %) chlorite (Savko et al., 2010).

As a temperature increased, bastnaesite started to decompose with the synthesis of monazite and eventually completely disappeared at the transition to the monazite zone. Monazite inclusions in bastnaesite of both morphological types (prismatic and acicular crystals and rosettes) (Figs. 5d, 5e) and the close association of bastnaesite, monazite, and apatite (Fig. 5c) testify that bastnaesite was formed by the reaction



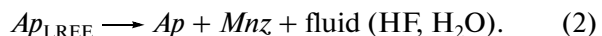
Similar relations between bastnaesite and monazite were documented in carbonaceous schists of the Timskaya Formation in the Tim–Yastrebovskii structure (Savko et al., 2010) and at the Bayan Obo Nb and REE deposit in Inner Mongolia, China (Smith et al., 1999).

Thus, reaction (1) corresponds to the isograde of bastnaesite decomposition (Bst-out isograde), and its temperature roughly corresponds to that of the staurolite-in isograde. Bastnaesite and allanite have never been found together in metapelites of the Vorontsovskaya Group, although these minerals are known to occur in association in carbonaceous schists of the Tim–Yastrebovskii structure of the Voronezh Crystalline Massif (Savko et al., 2010).

Monazite is present in all samples with REE-bearing minerals from the medium- and high-temperature metamorphic zones, and this mineral was identified in approximately half of our samples from the garnet zone (Table 5). This means that metamorphic monazite started to crystallize in the garnet zone, and its stability expands into higher temperature region (from the staurolite–sillimanite to sillimanite–potassic feldspar–cordierite zone).

In addition to reaction (1), monazite could be formed at the partial decomposition of chlorite, sillimanite breakdown, and at the sacrifice of REE-bearing apatite. Metapelites of the garnet metamorphic zone exhibit very unusual relations between monazite and chlorite (Figs. 7c–7e). Monazite replaces the margins and cores of chlorite flakes and forms small crystals (monazite dust, see Fig. 7d). Conceivably, analogous to bastnaesite, monazite crystallized at the partial decomposition of chlorite that contained REE.

Reaction relations between apatite and chlorite, such as monazite rims around apatite (Fig. 7b), thin monazite lamellas in apatite (Fig. 7a), monazite inclusions in apatite (Fig. 5f), suggest that monazite crystallized in the garnet (Figs. 5f, 7a) and staurolite (Fig. 7b) zones immediately from REE-rich apatite according to the reaction



This also follows from the fact that many apatite grains in the garnet and staurolite zones contain REE (up to 13.5 wt %) (Table 9). Moreover, the presence of F in some of the monazites (Table 7) suggests that they were formed at the expense of bastnaesite and/or apatite.

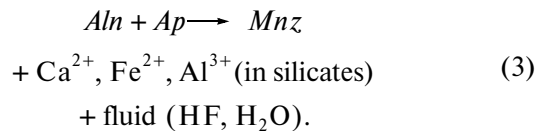
Although the most common reaction that synthesized monazite during metamorphism is thought to be

**Table 10.** Composition and cation proportions in the formula of xenotime from metapelites of the Vorontsovskaya Group

Component	548-c/4				8283/8				8358/1				8053/275				8312/1			
	8	10	8	9	10	3	4	5	33	34	35	36	37	16	41					
UO <sub>3</sub>	0.87	0.63	0.01	0.45	0.12	0.40	0.76	0.13	0.28	0.02	0.45	0.94	1.43	0.33	0.33					
P <sub>2</sub> O <sub>5</sub>	33.21	29.27	34.50	31.69	33.20	33.67	33.08	32.74	33.46	33.75	34.48	34.17	33.55	33.23	34.29					
SiO <sub>2</sub>	2.10	7.14	2.16	1.38	1.06	2.22	1.98	2.20	1.36	1.21	1.39	1.65	3.06	2.07	1.92					
ThO <sub>2</sub>	0.97	3.98	0.20	—	—	0.27	0.41	0.47	0.03	—	0.04	—	—	—	—					
Al <sub>2</sub> O <sub>3</sub>	—	1.62	0.78	—	0.01	—	0.04	0.06	—	—	—	0.12	0.07	0.07	0.10					
Y <sub>2</sub> O <sub>3</sub>	39.27	31.97	42.54	42.90	43.25	46.02	46.49	45.09	43.71	45.16	45.65	45.88	45.55	45.69	46.24					
La <sub>2</sub> O <sub>3</sub>	2.03	2.77	—	—	—	—	—	—	—	—	—	—	—	—	—					
Ce <sub>2</sub> O <sub>3</sub>	5.28	8.39	—	—	—	—	—	—	—	—	—	—	—	—	—					
Gd <sub>2</sub> O <sub>3</sub>	1.44	1.01	1.59	2.23	2.30	2.15	2.24	1.68	2.23	1.80	1.82	1.84	2.05	2.45	1.09					
Tb <sub>2</sub> O <sub>3</sub>	0.02	—	0.28	0.13	0.80	0.87	0.40	—	—	—	—	0.13	0.07	—	—	0.41				
Dy <sub>2</sub> O <sub>3</sub>	4.18	2.69	6.74	6.60	5.78	5.28	5.16	5.68	5.67	5.80	5.77	5.03	4.29	5.31	4.10					
Ho <sub>2</sub> O <sub>3</sub>	1.00	0.25	2.23	2.29	1.70	1.46	0.82	1.75	1.96	1.85	1.17	1.14	0.37	1.64	0.65					
Er <sub>2</sub> O <sub>3</sub>	3.57	3.34	3.42	4.42	4.83	3.78	3.79	5.29	4.37	4.88	3.76	4.40	4.27	3.61	3.03					
Yb <sub>2</sub> O <sub>3</sub>	4.00	2.89	5.47	6.78	5.50	2.55	3.45	3.26	4.09	4.40	3.50	4.51	3.13	2.86	5.40					
CaO	0.38	2.55	0.19	—	—	0.34	0.76	—	0.18	0.36	0.20	0.20	0.08	0.12	0.12					
PbO	0.37	0.63	—	0.46	0.41	0.27	0.14	0.36	0.50	—	0.16	—	0.01	0.43	0.55					
Total	98.69	99.13	99.83	99.48	98.29	98.6	99.43	99.81	98.1	98.9	97.88	99.6	97.61	98.87	98.23					
U	0.01	—	—	—	—	—	—	—	—	—	—	—	—	—	—	—	—			
P	0.95	0.80	0.95	0.92	0.96	0.94	0.92	0.91	0.91	0.96	0.97	0.95	0.93	0.94	0.96	0.06	—			
Si	0.07	0.23	0.07	0.05	0.04	0.07	0.07	0.07	0.07	0.05	0.04	0.05	0.05	0.05	0.07	0.06	—			
Th	0.01	0.03	—	—	—	—	—	—	—	—	—	—	—	—	—	—	—			
Al	—	0.06	0.03	—	—	—	—	—	—	—	—	—	—	—	—	—	—			
Y	0.71	0.55	0.74	0.78	0.78	0.81	0.82	0.79	0.79	0.80	0.81	0.80	0.80	0.81	0.81	—	—			
La	0.03	0.03	—	—	—	—	—	—	—	—	—	—	—	—	—	—	—			
Ce	0.07	0.10	—	—	—	—	—	—	—	—	—	—	—	—	—	—	—			
Gd	0.02	0.01	0.02	0.03	0.03	0.02	0.02	0.02	0.03	0.02	0.02	0.02	0.02	0.02	0.03	0.01	—			
Tb	—	—	—	—	—	0.01	0.01	—	—	—	—	—	—	—	—	—	—			
Dy	0.05	0.03	0.07	0.06	0.06	0.05	0.06	0.06	0.06	0.06	0.06	0.06	0.05	0.05	0.06	0.04				
Ho	0.01	—	0.02	0.02	0.02	0.01	0.02	0.02	0.02	0.02	0.02	0.01	0.01	—	0.02	0.01				
Er	0.04	0.03	0.04	0.05	0.05	0.04	0.04	0.05	0.05	0.05	0.05	0.05	0.04	0.04	0.04	0.03				
Yb	0.04	0.03	0.04	0.05	0.05	0.04	0.04	0.03	0.05	0.05	0.05	0.05	0.05	0.03	0.03	0.05				
Ca	0.01	0.09	0.01	—	—	—	—	0.01	0.03	—	0.01	0.01	0.01	0.01	—	—	—			
Pb	—	0.01	—	—	—	—	—	—	—	—	—	—	—	—	—	—	—			
SREE	0.97	0.78	0.93	1.00	0.99	1.00	0.98	0.99	1.00	0.98	0.99	1.00	0.98	0.94	0.99	0.95				

Note: Cation proportions were calculated by normalizing to a total of cations (2).

the high-temperature replacement of allanite by this mineral in the epidote-amphibolite facies (Wing et al., 2003; Janots et al., 2008; Janots et al., 2009; Tomkins and Pattison, 2007; and others), we found allanite only in two samples from the staurolite zone. The fact that the allanite contains P (Table 6, Fig. 5a) suggests that this mineral was synthesized at the sacrifice of detrital monazite, as was suggested in (Wing et al., 2003; Janots et al., 2008; and others). Allanite occurs in the form of small (relict) grains in association with apatite and monazite replaced by allanite (Figs. 5a, 5b). A number of reactions of the type  $Aln \longrightarrow Mnz$  was suggested in (Wing et al., 2003; Janots et al., 2008; Tomkins and Pattison, 2007); the reaction can be written in a general form as



An argument in support of the occurrence of this reaction is also provided by the drastic decrease (by a factor of almost three) in the LREE concentration in the decomposing allanite.

The grain size of apatite increases with increasing temperature from 10–20  $\mu\text{m}$  to 200  $\mu\text{m}$  in the sillimanite–potassic feldspar–cordierite zone.

Another REE phosphate, xenotime, is most widely spread in the staurolite–sillimanite zone. Its relations with other minerals were not examined in detail, and no conclusions can be drawn so far about reactions of its synthesis or decomposition. It is known from literature data that phase relations of xenotime in metapelites are closely coupled with growth and decomposition reactions of garnet, a mineral able to concentrate much Y and even be zonal in terms of concentration of this element (see, for example, Spear and Pyle, 2002).

## CONCLUSIONS

The following conclusions were drawn from phase relations of REE-bearing minerals in metasedimentary rocks of the Vorontsovskaya Group.

(1) Bastnaesite is the lowest temperature REE mineral and is stable only within the garnet zone. Bastnaesite can be formed in the greenschist facies at the recrystallization of detrital bastnaesite and the replacement of detrital monazite or at the partial decomposition of silicates (chlorite, biotite, and plagioclase) bearing REE in concentrations of a few dozen to a few hundred ppm, as follows from the diverse reaction textures.

(2) Reaction relations between bastnaesite, monazite, and apatite suggest that bastnaesite decomposes in the high-temperature part of the garnet zone with the synthesis of monazite according to the reaction  $Bst + Ap \longrightarrow Mnz + Ca^{2+}$  (in silicates) + fluid (HF,

$\text{CO}_2, \text{H}_2\text{O}$ ). This reaction is marked by the isograde of bastnaesite decomposition (*Bst-out*). The complete decomposition of bastnaesite coincides with the isograde of staurolite synthesis.

(3) Monazite first appears in the garnet zone and remains stable in all metamorphic zones, including the sillimanite–potassic feldspar–cordierite zone (in the lower part of the granulite facies). The diverse reaction textures suggest that the mineral is formed in the garnet zone by a reaction of bastnaesite with apatite at the partial decomposition of REE-bearing chlorite. Monazite is produced in the garnet and staurolite zones by a reaction of apatite with allanite and at the partial decomposition of REE-bearing apatite. The monazite stability field expands into the high-temperature region, including the granulite facies.

## REFERENCES

- Balashov, Yu.A., *Geokhimiya redkikh elementov* (Geochemistry of Trace Elements), Moscow: Nedra, 1976.
- Bibikova, E.V., Bogdanova, S.V., Postnikov, A.V., Popova, L.P., et al., Sarmatia–Volgo-Uralia Junction Zone: Isotopic-Geochronologic Characteristic of Supracrustal Rocks and Granitoids, *Stratigr. Geol. Korrelyatsiya*, 2009, no. 6, pp. 3–16 [*Stratigr. Geol. Correlation* (Engl. Transl.), no. 6, pp. 561–573].
- Chernyshov, N.M., Bayanova, T.B., Al'bekov, A.Yu., and Levkovich, N.V., New Data on the Age of Gabbro–Dolerite Intrusions of the Trap Formation in the Khoper Megablock, Voronezh Crystalline Massif, Central Russia, *Dokl. Akad. Nauk*, 2001, vol. 380, no. 5, p. 1–3 [*Dokl. Earth Sci.* (Engl. Transl.), vol. 380, pp. 889–891].
- Chernyshov, N.M., Ponomarenko, A.N., and Bartnitskii, E.N., New Age Data on Nickel-Bearing Differentiated Plutons in the Voronezh Crystalline Massif, *Dokl. Akad. Nauk SSSR, Ser. B.*, 1990, no. 6, pp. 11–19.
- Condie, K.C., Chemical Composition and Evolution of the Upper Continental Crust: Contrasting Results from the Surface Samples and Shales, *Chem. Geol.*, 1993, vol. 104, pp. 1–37.
- Corrie, S.L. and Kohn, M.J., Trace-Element Distributions in Silicates during Prograde Metamorphic Reactions: Implications for Monazite Formation, *J. Metam. Geol.*, 2008, vol. 26, pp. 451–464.
- Gerasimov, V.Yu. and Savko, K.A., Geospeedometry and Temperature Evolution of the Garnet–Cordierite Metapelites of the Voronezh Crystalline Massif, *Petrologiya*, 1995, vol. 3, no. 6, pp. 563–577.
- Gibson, D.H., Carr, S.D., Brown, R.L., and Hamilton, M.A., Correlations between Chemical and Age Domains in Monazite, and Metamorphic Reactions Involving Major Pelitic Phases: An Integration of ID-TIMS and SHRIMP Geochronology with Y–Th–U X-Ray Mapping, *Chem. Geol.*, 2004, vol. 211, pp. 237–260.
- Grew, E.S. and Manton, W.I., A New Correlation of Sapphirine Granulites in the Indo-Antarctic Metamorphic Terrain: Late Proterozoic Dates from the Eastern Ghats Province of India, *Precambrian Res.*, 1986, vol. 33, pp. 123–137.

- Hokada, T., Perrierite in Sapphirine-Quartz Gneiss: Geochemical and Geochronological Features and Implications for Accessory-Phase Paragenesis of UHT Metamorphism, *J. Miner. Petrol. Sci.*, 2007, vol. 102, pp. 44–49.
- Janots, E., Engi, M., Berger, A., Allaz, J., Schwarz, J.-O., and Spandler, C., Prograde Metamorphic Sequence of REE Minerals in Pelitic Rocks of the Central Alps: Implications for Allanite–Monazite–Xenotime Phase Relations from 250 to 610°C, *J. Metam. Geol.*, 2008, vol. 26, pp. 509–526.
- Janots, E., Engi, M., Rubatto, D., Berger, A., Gregory, C., and Rahn, M., Metamorphic Rates in Collisional Orogeny from in Situ Allanite and Monazite Dating, *Geology*, 2009, vol. 37, no. 1, pp. 11–14.
- Kelly, N.M., Clarke, G.L., and Harley, S.L., Monazite Behavior and Age Significance in Poly-Metamorphic High-Grade Terrains: A Case Study from the Western Musgrave Block, Central Australia, *Lithos*, 2006, vol. 88, pp. 100–134.
- Kohn, M.J. and Malloy, M.A., Formation of Monazite via Prograde Metamorphic Reactions among Common Silicates: Implications for Age Determinations, *Geochim. Cosmochim. Acta*, 2004, vol. 68, no. 1, pp. 101–113.
- Lanzirotti, A. and Hanson, G.N., Geochronology and Geochemistry of Multiple Generations of Monazite from the Wepawaug Schist, Connecticut, USA: Implications for Monazite Stability in Metamorphic Rocks, *Contrib. Mineral. Petrol.*, 1996, vol. 125, pp. 332–340.
- Lebedev, I.P., Reconstruction of Primary Nature and Conditions of Prograde Metamorphism of the Early Proterozoic Complexes of the Vorontsovskaya Formation, *Extended Abstract of Cand. (Geol-Miner.) Dissertation*, Voronezh, 1977.
- Likhonov, I.I., Reverdatto, V.V., and Vershinin, A.E., Fe- and Al-Rich Metapelites of the Teiskaya Group, Yenisei Range: Geochemistry, Protoliths, and the Behavior of Their Material during Metamorphism, *Geokhimiya*, 2008, no. 1, pp. 20–41 [*Geochem. Int.* (Engl. Transl.), no. 1, pp. 17–36].
- McFarlane, C.R.M., Connelly, J.N., and Carlson, W.D., Monazite and Xenotime Petrogenesis in the Contact Aureole of the Makhavinek Lake Pluton, Northern Labrador, *Contrib. Mineral. Petrol.*, 2005, vol. 148, pp. 524–541.
- McLennan, S.M., Hemming, S.R., Taylor, S.R., and Eriksen, R.E., Early Proterozoic Crustal Evolution: Geochemical and Nd–Pb Isotopic Evidence from Metasedimentary Rocks, Southwestern North America, *Geochim. Cosmochim. Acta*, 1995, vol. 59, no. 6, pp. 1153–1177.
- Murrey, R.W., Buchholtz, Ten., Brink, M.R., Jones, D.L., et al., Rare Earth Elements as Indicator of Different Marine Depositional Environments in Chert and Shale, *Geology*, 1990, vol. 18, pp. 268–272.
- Polyakova, T.N., Savko, K.A., and Skryabin, V.Yu., Petrologiya metapelitov i silikatno-karbonatnykh porod Tim-Yastrebovskoi struktury (Voronezhskii kristallicheskii massiv), in *Trudy NII Geologii VGU* (Petrology of Metapelites and Calc–Silicate Rocks of the Tim-Yastrebovskii Structure, Voronezh Crystalline Massif), Voronezh: Izd-vo Voronezhskogo un-ta, 2006, no. 35.
- Rasmussen, B. and Muhling, J.R., Monazite Begets Monazite: Evidence for Dissolution of Detrital Monazite and Reprecipitation of Syntectonic Monazite during Low-Grade Regional Metamorphism, *Contrib. Mineral. Petrol.*, 2007, vol. 154, pp. 675–689.
- Savko, K.A. and Gerasimov, Yu.V., *Petrologiya i geospodemetriya metamorficheskikh porod vostoka Voronezhskogo kristallicheskogo massiva* (Petrology and Geospeedometry of the Metamorphic Rocks of the Eastern Voronezh Crystalline Massif), Voronezh, 2002.
- Savko, K.A., Korish, E.Kh., Pilyugin, S.M., and Polyakova, T.N., Phase Relations of REE-Bearing Minerals during the Metamorphism of Carbonaceous Shales in the Tim–Yastrebovskaya Structure, Voronezh Crystalline Massif, Russia, *Petrologiya*, 2010, vol. 18, no. 4, pp. 402–433 [Petrology (Engl. Transl.), vol. 18, no. 4, pp. 384–415].
- Savko, K.A., Low-Temperature Rocks in Metamorphic Zoning of the Vorontsovskaya Group of VCM, *Geol. Geofiz.*, 1994a, no. 3, pp. 50–59.
- Savko, K.A., Sillimanite–Muscovite Zone in the Metamorphic Complex of the Vorontsovskaya Group of VCM, *Geol. Geofiz.*, 1994b, no. 6, pp. 73–86.
- Savko, K.A., Zoning of Minerals and Prograde Metamorphic Reactions in the Moderate-Temperature Metapelites of the Vorontsovskaya Group, Voronezh Crystalline Massif, *Izv. Akad. Nauk SSSR, Ser. Geol.*, 1990, no. 11, pp. 79–87.
- Shchipanskii, A.A., Samsonov, A.V., Petrova, A.Yu., and Larionova, Yu.O., Geodynamics of the Eastern Margin of Sarma-tia in the Paleoproterozoic, *Geotektonika*, 2007, no. 1, pp. 43–70 [Geotectonics (Engl. Transl.), no. 1, pp. 38–62].
- Smith, H.A. and Barero, B., Monazite U–Pb Dating of Staurolite Grade Metamorphism in Pelitic Schists, *Contrib. Mineral. Petrol.*, 1990, vol. 105, pp. 602–615.
- Smith, M.P., Henderson, P., and Peishan, Z., Reaction Relationships in the Bayan Obo Fe–REE–Nb Deposit, Inner Mongolia, China: Implications for the Relative Stability of Rare-Earth Element Phosphates and Fluorocarbonates, *Contrib. Mineral. Petrol.*, 1999, vol. 134, pp. 294–310.
- Spear, F.S. and Pyle, J.M., Apatite, Monazite, and Xenotime in Metamorphic Rocks, *Rev. Mineral. Geochem.*, 2002, vol. 48, pp. 293–335.
- Suzuki, K., Adachi, M., and Kajizuka, I., Electron Microprobe Observations of Pb Diffusion in Metamorphosed Detrital Monazites, *Earth Planet. Sci. Lett.*, 1994, vol. 128, pp. 391–405.
- Tomkins, H.S. and Pattison, D.R.M., Accessory Phase Petrogenesis in Relation to Major Phase Assemblages in Pelites from the Nelson Contact Aureole, Southern British Columbia, *J. Metam. Geol.*, 2007, vol. 25, pp. 401–421.
- Wing, B.A., Ferry, J.M., and Harrison, T.M., Prograde Destruction and Formation of Monazite and Allanite during Contact and Regional Metamorphism of Pelites: Petrology and Geochronology, *Contrib. Mineral. Petrol.*, 2003, vol. 145, pp. 228–250.